The CO_2 consumption potential during gray shale weathering: Insights from the evolution of carbon isotopes in the Susquehanna Shale Hills critical zone observatory

Lixin Jin [a,*], Nives Ogrinc [b], Tiffany Yesavage [c], Elizabeth A. Hasenmueller [d,1], Lin Ma [a], Pamela L. Sullivan [c], Jason Kaye [d], Christopher Duffy [e], Susan L. Brantley [c]

[a] *Department of Geological Sciences, University of Texas at El Paso, El Paso, TX, USA*
[b] *Department of Environmental Sciences, Jozef Stefan Institute, Ljubljana, Slovenia*
[c] *Earth and Environmental Systems Institute, Department of Geological Sciences, Pennsylvania State University, State College, PA, USA*
[d] *Department of Ecosystem Science and Management, Pennsylvania State University, State College, PA, USA*
[e] *Department of Civil Engineering, Pennsylvania State University, State College, PA, USA*

Abstract

Shale covers about 25% of the land surface, and is therefore an important rock type that consumes CO_2 during weathering. We evaluated the potential of gray shale to take up CO_2 from the atmosphere by investigating the evolution of dissolved inorganic carbon (DIC) concentrations and its carbon isotopic ratio ($\delta^{13}C_{DIC}$) along water flow paths in a well-characterized critical zone observatory (Susquehanna Shale Hills catchment). In this catchment, chemical weathering in shallow soils is dominated by clay transformation as no carbonates are present, and soil pore waters are characterized by low DIC and pH. In shallow soil porewaters, the DIC, dominated by dissolved CO_2, is in chemical and isotopic equilibrium with CO_2 in the soil atmosphere where pCO_2 varies seasonally to as high as 40 times that of the atmosphere. The degradation of ancient organic matter is negligible in contributing to soil CO_2. The chemistry of groundwater varies along different flowpaths as soil pore water recharges to the water table and then dissolves ankerite or secondary calcite under the valley floor. Weathering of carbonate leads to much higher concentrations of DIC ($\sim$2500 μmol/L) and divalent cations (Ca^{2+} and Mg^{2+}) in groundwaters than soil waters. The depth to the ankerite weathering front is hypothesized to be roughly coincident with the water table but it varies due to heterogeneities in the protolith composition. Groundwater chemistry therefore shows different saturation indices with respect to ankerite depending upon location along the valley. The $\delta^{13}C_{DIC}$ values of these groundwaters document mixing between the ankerite and soil CO_2. The major element concentrations, DIC, and $\delta^{13}C_{DIC}$ in the first-order stream incising the valley of the catchment are derived from groundwater and soil waters in proportions that vary both spatially and temporally. The CO_2 degassed slightly in the stream but little evidence of C isotopic equilibration with the atmosphere is observed, due to the short length of the stream and short contact time with air.

The ankerite reaction front also lies close to the pyrite dissolution front. Pyrite oxidation in bedrock likely released sulfuric acid and played a minor role in the ankerite dissolution, shifting groundwater $\delta^{13}C_{DIC}$ slightly above the expected mixing values. At the catchment scale, the stream SO_4^{2-} is also dominantly derived from wet deposition, as stream has $\delta^{34}S_{SO4}$ values around 3‰, well within the range of acid deposition.

---

* Corresponding author. Tel.: +1 915 747 5559; fax: +1 915 747 5073.
E-mail address: ljin2@utep.edu (L. Jin).
[1] Current address: Department of Earth & Atmospheric Sciences, Saint Louis University, Saint Louis, MO, USA.

A mass balance calculation shows that silicate and ankerite dissolution of the Rose Hill shale at Shale Hills consumes CO_2 at a rate of $\sim$44 and $\sim$42–48 mol m^{-2} ky^{-1} respectively, while degradation of ancient organic matter releases CO_2 at a rate of $\sim$1.3 mol m^{-2} ky^{-1}. Silicate dissolution at the shallow soils is facilitated by low pH and high soil pCO_2. As ankerite dissolution and organic matter oxidation are shown to occur early during shale alteration, CO_2 consumption by shale weathering is thus limited by initiation of rock disintegration (e.g., fractures) and exposure of fresh surface area to infiltrating CO_2- and O_2-rich water.

1. INTRODUCTION

Chemical weathering transforms bedrock into soils at the Earth's surface, and these reactions take up atmospheric CO_2 and control inorganic carbon fluxes in hydrological systems. On global scales, an important negative feedback between continental weathering and global average surface temperature entails the consumption of CO_2 through dissolution of silicate minerals and transport of dissolved inorganic carbon (DIC) to the oceans, where most CO_2 is ultimately isolated from the active carbon pool by carbonate precipitation (Holland, 1978; Berner and Berner, 1996; Williams et al., 2007; Szramek et al., 2007). Dissolution rates of silicate minerals are elevated at higher atmospheric temperatures, leading to more sequestration of atmospheric CO_2, and thus lower atmospheric temperature. This negative feedback has been modeled based on investigations of the major silicate rock types (Amiotte-Suchet et al., 2003). However, few studies have focused on shale even though it is ubiquitous and represents as much as 25% of continental land area.

Amiotte-Suchet et al. (2003) concluded that shale might account for as much as 40% of the global annual soil/atmospheric CO_2 consumption during weathering, probably partly due to the presence of carbonate minerals in shales (e.g., as inter-bedded carbonate layers). The potential for carbonate mineral weathering to sequester CO_2 differs from that of silicate minerals because carbonate mineral weathering products are subject to eventual re-precipitation and release of CO_2 in approximately the same proportion to that which was sequestered over geological timescales (e.g., Ridgwell and Edwards, 2007). Thus it is important that we can separate the contribution of dissolution of silicates from carbonates during shale weathering, and identify the C sources.

Stable C isotope ratios ($\delta^{13}C$) are commonly used to identify C sources because of distinctively different ratios observed in major C reservoirs: $\sim$0‰ for marine carbonate, $\sim$−8.0‰ for atmospheric CO_2, and −27‰ to −12‰ for organic matter (based on C_3 and C_4 assimilation pathways during photosynthesis, respectively) (Friedli et al., 1986; Vogel, 1993; Yang et al., 1996; Telmer and Veizer, 1999; Karim and Veizer, 2000; Hélie et al., 2002; Allison et al., 2003; Singh et al., 2005; Jin et al., 2010). The $\delta^{13}C$ values of respired CO_2 in soil depend largely on the organic carbon (OC) sources. The $\delta^{13}C$ values of soil CO_2 become slightly heavier due to soil gas diffusion which preferentially removes lighter C isotopes or mixing with atmospheric CO_2 (Hillaire-Marcel, 1986; Ehleringer et al., 1991; Vogel, 1993;

Jin et al., 2010). Consequently, DIC in natural waters shows a wide range of C isotopic ratios that are controlled by the C sources as well as the kinetic and equilibrium fractionation factors.

In addition to carbonic acid (dissolved CO_2), sulfuric, nitric or organic acids are also key dissolution agents that drive silicate and carbonate weathering. However, reactions with these acids do not take up CO_2, and thus are not involved in Earth's climate-weathering negative feedback. In contrast, strong acid can react with carbonate rocks to release CO_2. For example, dissolution of liming material by strong acids derived from fertilizers in farmlands has been shown to be an important source of greenhouse gas to the atmosphere (Raymond and Cole, 2003; Hamilton et al., 2007).

Shales are known to contain pyrite that dissolves oxidatively to produce sulfuric acid. However, contribution of the sulfuric, instead of carbonic acid to chemical weathering reactions is hard to quantify using only elemental stoichiometry. This is because sulfate (SO_4^{2-}) in natural waters can also derive from atmospheric deposition, and this SO_4^{2-} is not necessarily involved in chemical weathering reactions. Similar to C isotopes, the $\delta^{34}S_{SO4}$ of soil water, groundwater and riverine SO_4^{2-} is an environmental tracer because of the large natural variation of $\delta^{34}S$ observed in different S-bearing reservoirs such as sulfide, gypsum, and S-containing coals (Lueth et al., 2005; Cambell and Lueth, 2008). The range of $\delta^{34}S$ isotope ratios in anthropogenic sulfur in acid rain is narrow, constrained between −1‰ and 6‰ (Wadleigh et al., 1994; Benkovitz et al., 1996; Alewell et al., 2000; Herut et al., 2005). When SO_4^{2-} is rapidly immobilized in the soils, the fractionation of the S isotopes has been shown to be negligible (Trust and Fry, 1992). In shale, sulfides are generally present as pyrite and their $\delta^{34}S$ values range from −20‰ to 15‰ (Migdisov et al., 1983; Strauss, 1999). Since the geochemical reactions of weathering and oxidation cause only small S isotope fractionations in hydrological systems, the $\delta^{34}S_{SO4}$ pinpoints with high accuracy the primary sources of S and the rock formations undergoing water–rock interaction (Krouse and Grinenko, 1991; Clark and Fritz, 1997).

The global inventory of carbon as OC in sedimentary rocks is greater than all the other surface reservoirs combined (oceans, soils, biomass and atmosphere) (Hedges and Oades, 1997; Petsch et al., 2001; Jaffe et al., 2002; Copard et al., 2007). Shale, especially black shale with an average of 1 wt% OC, stores the majority of the fossil OC (Copard et al., 2007). Although most of the ancient organic matter in sedimentary rocks is relatively refractory, it is

susceptible to alteration at Earth's surface (e.g., Clayton and Swetland, 1978; Littke et al., 1991; Keller and Bacon, 1998; Petsch et al., 2000; Jaffe et al., 2002; Jin et al., 2013). The fossil organic matter is lost by biogeochemical weathering through oxidation, hydrolysis and microbial consumption (Copard et al., 2007). It is important to understand the fate of organic matter during chemical weathering as this transformation reaction releases CO_2 and consumes O_2 levels on global scales (Petsch et al., 2000; Sageman et al., 2003; Petsch et al., 2005).

Here we present a study of inorganic and organic carbon dynamics in central Pennsylvania soils developed on gray shale of the Silurian Rose Hill Formation at the Susquehanna Shale Hills critical zone observatory (SSHO). With carbonate minerals completely leached in the shallow horizons, the reaction front for carbonate weathering lies at depth in the bedrock, offering the opportunity to determine the relative contribution of DIC from carbonate mineral C versus soil CO_2. Likewise, degradation of modern vegetation occurs in the soil whereas oxidation of fossil organic matter occurs in bedrock at depth. Lastly, pyrite is present and reactive at SSHO, and its weathering front is inferred to lie at depth roughly parallel with that of carbonates near the ridge site. So a transition is expected for the sources of sulfuric acid, where acid rain dominates the signal at the soil surface and pyrite dissolution dominates at depth. These features make SSHO an ideal field site to study C transformation processes among OC, soil CO_2 and DIC in natural waters as well as carbonic versus sulfuric acid weathering pathways during shale weathering.

In this study our main goal is to quantify the release rates of CO_2 from decomposition of fossil carbon and consumption rates of CO_2 from shale weathering, and thus evaluate the net CO_2 consumption potential of gray shale. Toward that end, we: (1) evaluate the relative contribution of "old" versus "modern" organic matter sources to soil CO_2; (2) study the controls on DIC acquisition as water passes through the vadose zone to a shallow aquifer and to a first-order stream; and (3) investigate the sources of dissolved SO_4^{2-} at the Shale Hills watershed, and quantify the relative importance of sulfuric acid versus carbonic acid weathering. This case study leads to better understanding of the weathering of individual minerals, and places important constraints on shale's potential to consume CO_2, especially for shale containing only trace carbonate minerals.

2. STUDY AREA

Susquehanna Shale Hills critical zone observatory (SSHO) is an 8-ha catchment, located in central Pennsylvania, and with mean annual temperature of 10 °C and mean annual precipitation of 107 cm according to long-term climate record (NOAA, 2007). The hydrology and hydrochemistry of the SSHO have been well studied. The hydrological processes and responses of this catchment have been well characterized through monitoring and modeling (Qu and Duffy, 2007; Graham and Lin, 2011; Jin et al., 2011; Thomas et al., 2013). Precipitation is evenly distributed throughout the year, but also characterized by

large intermittent storms. The V-shaped catchment has a 1st-order ephemeral stream with a channel generally aligned from east to west in the valley (Fig. 1). The stream discharge is dominated by snowmelt in early spring and rainstorms in the fall. It dries out in the summer due to enhanced evapotranspiration, except for during major storms. The depths to water table in the wells next to the stream fluctuate seasonally, ~1.5 m in the summer and dry months, and approach or rise above the ground surface in the wetter spring and fall seasons (Brantley et al., 2013). Our sampling campaign focused on spring and late fall, the two seasons with high discharge and thus major elemental fluxes out of the catchment.

The catchment is hydrologically responsive, and the peaks in stream discharge are observed less than a week after a major rainfall event. This is attributed to preferential flowpaths and the macropores which have been identified within soils or possibly due to fractures within underlying saprock (Lin, 2006; Jin et al., 2011; Kuntz et al., 2011). Indeed, the residence time of soil water and groundwater was estimated to be less than one year from H/O isotope data (Jin et al., 2011). The soil waters are hydrologically closely connected to the shallow groundwaters, and the stream. The stream receives contributions mainly from groundwater during the warmer months characterized by low discharge and by soil waters during high discharge seasons. Thus, the stream chemistry has been shown to vary seasonally (with discharge) (Jin et al., 2011). Approximately 50% of annual precipitation is lost through evapotranspiration, while the other 50% leaves as stream discharge (Jin et al., 2011).

The catchment is developed almost entirely upon Silurian Rose Hill shale (Clinton group; Folk, 1960; Lynch, 1976; Lynch and Corbett, 1985), consisting of olive-pink to grayish-buff shale with a few layers of interbedded limestone (Lynch, 1976). Previous geochemical studies at SSHO have focused on isotopic, elemental and mineralogical observations (Jin et al., 2010, 2011; Herndon et al., 2011; Ma et al., 2011; Yesavage et al., 2012; Brantley et al., 2013). The silicate fraction of the bedrock underlying the SSHO contains mainly quartz and clays (illite and chlorite), with trace amounts of feldspar, pyrite and organic matter. Various amounts of ankerite are observed only deep in the subsurface. In the Rose Hill shale bedrock, about 0.1% S is observed in the form of pyrite; in contrast, the soils contain only ~0.01 wt% S. Several weathering reactions at the northern ridge are observed (from deep to shallow): pyrite dissolution at 23 m depth, ankerite (Fe, Mn-rich dolomite) dissolution at ~22 m depth, plagioclase dissolution at ~4–5 m depth, and clay mineral dissolution at ~0.5 m depth (Jin et al. 2010; Jin et al., 2011; Brantley et al., 2013). The depths to weathering fronts for pyrite and carbonates, however, are much shallower at the valley floor locations (Brantley et al., 2013). At SSHO, relatively unfractured and chemically/mineralogically unaltered shale is defined as 'bedrock' (below 23 m at northern ridge); the in-place rock that is somewhat fractured and geochemically altered to a small extent is defined as 'saprock' (23 to 0.5 m at northern ridge); the unconsolidated and highly weathered materials that are augerable are
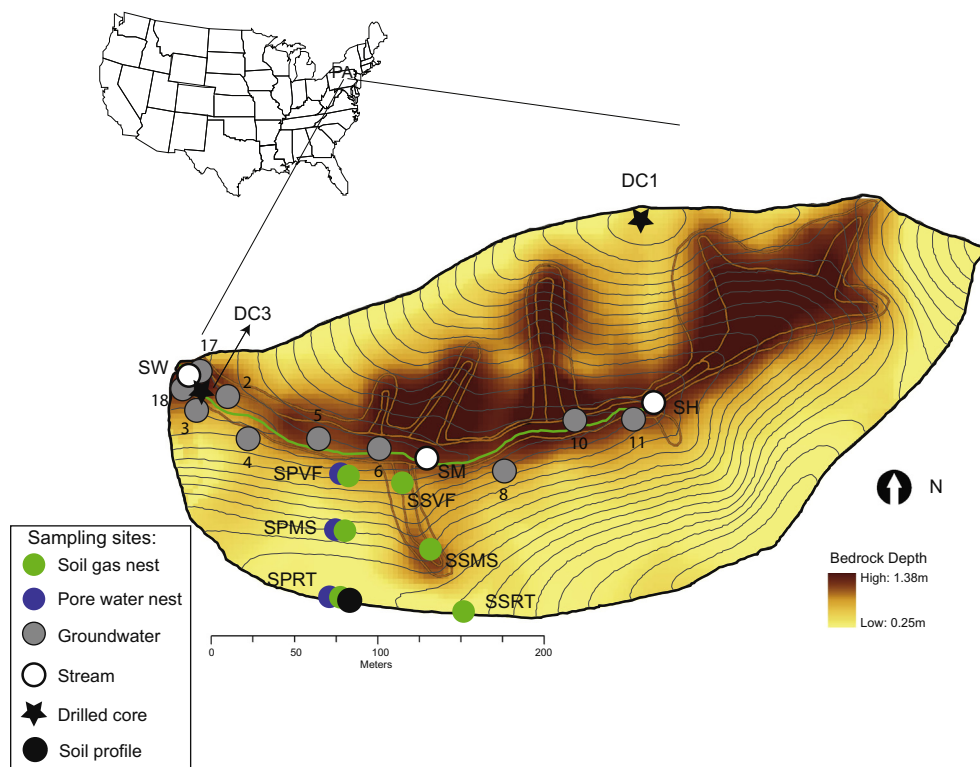
Fig. 1. Sample locations on a depth-to-bedrock map of the Susquehanna Shale Hills critical zone observatory (SSHO; Lin, 2006). Water samples include soil water from nested lysimeters at three sites along a southern planar transect (SPRT, SPMS, and SPVF; blue circles), river waters at three locations along the first order stream (SH, SM and SW; white circles), and groundwaters at 10 wells along the valley (well #2, 3, 4, 5, 6, 8, 10, 11, 17, 18; grey circles). Soil gas samples were collected at different depths at the SPRT, SPMS and SPVF sites as well as three sites along a southern swale transect (SSRT, SSMS and SSVF) (green circles). Soil CO_2 effluxes were measured at 7 locations along the southern planar transect and at 9 locations along the southern swale transect. Solid samples include archived soils from the SPRT site (black circle) and drilled core samples from DC1 and DC3 (black stars). (For interpretation of the references to color in this figure legend, the reader is referred to the web version of this article.)

termed as 'soil' (0.5 m to soil surface). Soil thickness varies with landscape location in the catchment, with thinner soils at the ridge top and thicker soils in the valley floor and in topographic depressions (Fig. 1; Lin, 2006).

The SSHO is a forested catchment, with oak (63% of total basal area), hemlock (16%), hickory (13%), and pines (8%) as the dominant species (Wubbels, 2010). Deciduous trees (maple and oak) cover the slopes while hemlocks and pines are present in the valley (Lin, 2006). The SSHO was recently logged in the 1930s. Organic matter content in different landscape locations and DOC in soil waters, groundwaters and streams have been investigated (Andrews et al., 2011). Degradation of organic matter and thus subsequent release of DOC and CO_2 are more important within the swales, where soils are thicker and more hydrologically active (Andrews et al., 2011; Hasenmueller et al., 2014).

The SSHO is a relatively pristine watershed, but has been impacted by minor recent industrial pollution. Evidence for such anthropogenic contamination includes enrichment of Mn and Pb at the soil surface from steel and ferroalloy manufacturing, gasoline additives, and coal combustion (Herndon et al., 2011; Ma et al., 2014). The SSHO is also impacted by acid deposition. The

biogeochemistry of S derived from acid rain has been intensively studied in the soils of northeastern USA (Nordstrom, 1982; Ulrich and Pankrath, 1983; Reuss and Johnson, 1986; Mayer et al., 1995; Sharpe and Drohan, 1999; Canfield, 2001). It has been shown that the residence time of S in soils is longer than several months because of adsorption of sulfate to Fe oxyhydroxide and clays, precipitation as Al-hydroxy sulfate minerals, or/and microbial sulfate mineralization (Fitzgerald, 1976; Rajan, 1978; Nordstrom, 1982; Khanna et al., 1987; Mayer et al., 1995).

3. METHODS

3.1. Collection of water, gas and solid samples

Nests of lysimeters (tension soil water samplers) were installed in 2006 at three sites along a planar transect on the southern slope of the watershed: the ridge top (SPRT), mid-slope (SPMS) and valley floor (SPVF) (Fig. 1; details in Jin et al. 2011; Andrews et al., 2011). One day to one week prior to sampling these lysimeters, a vacuum of 0.5 bar was applied to draw water into the ceramic cups. Groundwater samples at the SSHO were collected from ten wells along the valley floor (Fig. 1). These wells, cased

to ~3 m below land surface, are situated in the shallow aquifers and linked hydrologically and geochemically to the soil waters and streams. The first-order ephemeral stream water was sampled at three locations: SH at the headwater, SM near the mid-point, and SW by the old weir at the outlet of the catchment (Fig. 1).

Soil water, groundwater and stream samples were collected three times: November 2011, May 2012 and April 2013, when the soils were wet and stream discharge was high. Groundwater and stream samples were filtered through 0.45 μm Whatman polypropylene filters. Ceramic cups of lysimeters have a maximum pore size of 1.3 μm, so soil waters were not further filtered. A previous study at SSHO has shown that further filtration to <0.45 μm does not change the concentrations of major ions, such as Mg^{2+}, Ca^{2+}, and sulfate, but does lower those of relatively insoluble elements such as Fe and Al (Yesavage et al., 2012). Thus, it is reasonable to assume that Ca^{2+} etc is predominantly in the dissolved form, while Fe and Mn in soil waters are partially lost via colloidal transport. One aliquot of each water sample was stored in pre-cleaned HDPE bottles and acidified with high-purity nitric acid for cation analyses. Another filtered aliquot was left untreated for alkalinity titrations, anion analyses and S isotopes. Samples for the stable isotope analyses of DIC were stored in glass bottles, capped with a stopper leaving no headspace and subsequently crimped to avoid any exchange with atmosphere. All samples were stored at 4 °C until analysis.

Nests of soil gas tubes were installed at the SPRT, SPMS and SPVF sites in 2008, following a modified USGS protocol, at 10 or 20 cm depth intervals until the depth of refusal during augering. Specifically, the tubes consisted of 1/8-inch ID stainless steel tubing with one end wrapped by stainless steel mess to keep soil materials from clogging the tubing. The other end is fit with a Swagelok® cap. Another three nests of soil gas tubes were installed at a southern swale transect in 2009 (Fig. 1): the ridge top (SSRT), mid-slope (SSMS) and valley floor (SSVF). The soil gas samples were collected in the field using 60-mL plastic syringes and needles after purging to clear the sampler tube. Gas samples were immediately transferred to 15 mL Labco®pre-evacuated glass vials. Soil gas CO_2 samples were collected twice over the study period (June 2012 and April 2013). Soil gas samples for $\delta^{13}C$ analysis were collected in the same way as CO_2 concentration samples.

Solid samples were collected previously and archived, including soils at SPRT as well as weathered and unweathered rocks from a drilled core (DC1) at the northern ridge (Fig. 1; Jin et al., 2010). By combining soils, saprock and bedrock samples from DC1, we have a complete weathering profile.

3.2. Analyses of solid samples

Solid samples, including soil and rock, were air-dried at room temperature for a week, then ground to pass a 100-mesh sieve (150 μm). Total OC contents of these samples have been reported previously (Jin et al., 2010). Soil and rock samples for C isotope measurements in OC ($\delta^{13}C_{OC}$) were combusted in an elemental analyzer (Costech) and

measured on a continuous-flow isotope ratio mass spectrometer (IRMS; Finnigan Delta PlusXL). Precision for $\delta^{13}C_{OC}$ is ±0.1‰ or better (1σ). In order to measure C isotope composition of the carbonate minerals ($\delta^{13}C_{Ca}$), soil or rock samples were reacted with dehydrated H_3PO_4 under vacuum at 70 °C. The released CO_2 was then measured by an IRMS (Finnigan MAT 252). For these measurements, precision is better than ±0.08‰ (1σ).

3.3. Analyses of gas samples

Soil gas CO_2 concentrations (pCO$_2$) were measured by a LiCOR 7000, calibrated with CO_2 standards with concentrations of 970 and 10300 ppmv. The isotopic composition of soil CO_2 was determined using a Europa 20–20 continuous flow IRMS with an ANCA TG preparation module for trace gas samples. Gas samples were flushed with He across two chemical traps that removed water and then trapped the CO_2. The isotope ratios of soil gas samples were analyzed at the Jozef Stefan Institute in Slovenia. Precision is better than ±0.1‰ (1σ), based on repeated internal standards.

In addition to soil gas sample collection, a LICOR 6200 analyzer was attached to a respiration chamber to measure CO_2 efflux in-situ at the SPRT, SPMS and SPVF sites (details on data collection are reported in Hasenmueller et al. (2014)).

3.4. Analyses of water samples

Water pH was measured in the field using a Corning 315 portable pH meter and a Ross glass-body combination pH electrode calibrated on the NBS scale using two low-ionic-strength buffer solutions (4 and 7). With the vacuum applied to the lysimeters during the sampling period, degassing could not be totally avoided. The pH values measured are thus the maximum values, and the estimated uncertainty is ±0.05 units. Water temperature was immediately measured after sample collection.

Concentrations of major cations, (Ca, Mg, Na, K, Sr, Fe, Mn) and anions (Cl, nitrate, and sulfate) as well as silica were measured with a Perkin Elmer inductively coupled plasma optical emission spectrometer (ICP-OES, DV5300) and Dionex-2100 ion chromatograph (IC), respectively at the Low-Temperature Geochemistry Laboratory of the University of Texas at El Paso (UTEP). The precision of ICP-OES and IC analyses was better than ±3% for major elements and ±10% for minor elements. Total alkalinity was determined on refrigerated water samples by weak hydrochloric acid titration using Mettler Toledo DL15 auto-titrator and data reanalyzed using the Gran alkalinity method (Edmond, 1970; Gieskes and Roders, 1973; Stumm and Morgan, 1996). Alkalinities of water samples from November 2011 and May 2013 were not titrated, but calculated based on charge balance. The uncertainty for alkalinity titrations is ±10% for most of groundwater and stream samples, but much higher for soil water, groundwater and stream samples with very low alkalinity values. Uncertainties were estimated by comparing measured and calculated alkalinity values where both were available.

The mineral saturation states and pCO$_2$ concentrations of the water samples were calculated using the USGS program Solmineq.88 (Kharaka et al., 1988) using measured major ion concentrations, dissolved silica content, pH and alkalinity. For most groundwater samples, alkalinity was not measured and estimated based on charge balance. For samples where temperature was not measured in the field, a temperature of 10 °C, the mean annual air temperature, was assumed for groundwaters, and mean daily air temperature for a given sample date (monitored by the weather station at SSHO) was assumed for soil water and stream water samples. The saturation index, SI, is defined as log (IAP/Ksp) where IAP and Ksp are the ion activity product of mineral dissolution reaction and the solubility constant of the mineral, respectively. Positive SI values indicate the water is supersaturated with respect to a given mineral, while negative values indicate the water is undersaturated with respect to a given mineral. The SI values for both calcite and dolomite were used as proxies of ankerite saturation. Given the likely variability in pH and temperature, the saturation index estimates were assumed to be only reliable within ±0.5 log units.

The stable isotope composition of dissolved inorganic carbon ($\delta^{13}C_{DIC}$) was determined with an IRMS (Thermo-Quest Finnigan Delta PlusXL) coupled with a Gasbench automated sampler (also manufactured by Finnigan). Samples were reacted for >1 h with phosphoric acid at room temperature in vials previously flushed with He gas. The dissolved sulfate in water samples was precipitated as BaSO$_4$ and its isotope composition ($\delta^{34}S_{SO4}$) was measured as SO$_2$ gas in a continuous-flow gas-ratio mass spectrometer (ThermoQuest Finnigan Delta PlusXL). Precision is estimated to be ±0.15 or better (1σ), based on repeated internal standards.

All stable isotope measurements of C and S isotope ratios of water samples were commercially analyzed by the Environmental Isotope Laboratory at the University of Arizona. Results are expressed in the conventional delta (δ) notation, defined as per mil (‰) deviation from reference standard VPDB and CDT.

4. RESULTS

4.1. Carbon content and isotopic composition of solid samples

The C isotopic compositions of solid samples, including organic carbon in the soils, drilled bedrock samples, and carbonate minerals in the drilled bedrock are reported in Table 1. Also included are organic and inorganic carbon contents, published previously for the same samples (Jin et al., 2010). The organic carbon (OC) concentrations of the DC1 core samples, previously published for the same samples in Jin et al. (2010), ranges from 0.03 to 0.05 wt%, much lower than those of the shallow soils where carbon is mainly derived from modern vegetation (Table 1; Fig. 2A). For example, for the soil profile SPRT, OC concentrations are almost 1.8 wt% at surface but decrease sharply with depth.

The $\delta^{13}C_{OC}$ values of the DC1 samples are variable (−27.3‰ to −25.9‰), but more negative than those of soils (−25.8‰ to −25.3‰) (Table 1; Fig. 2B). When the OC concentrations are plotted versus the isotopic compositions two clusters are defined, delineating the ancient and modern organic carbon sources (Fig. 2C). The $\delta^{13}C_{OC}$ values of the soils increase with depth (Fig. 2C). Only the two bottom-most samples in the DC1 drill core contain measurable amounts of the carbonate mineral ankerite (1.5–7.8 wt%) (Table 1). The ankerite has C isotope ratios averaging −5.9 ± 0.3‰ (n = 2). One sample from another core derived from borehole DC3 drilled in the valley (Fig. 1), contains calcite with a $\delta^{13}C_{Ca}$ value of −1.1‰, different from that of the DC1 core (Table 1).

Table 1
$\delta^{13}C$, organic carbon and ankerite concentrations in SSHO soil and rock samples.

Sample depth (m)	OC[a] wt%	Ankerite[a] wt%	$\delta^{13}C$ (‰) OM	$\delta^{13}C$ (‰) carbonate	$\delta^{13}C$ (‰)[b] total carbon	Total carbon[b] wt%
Soil profile: SPRT						
0.05	1.76	0	−25.8			
0.15	0.79	0	−25.6			
0.25	0.37	0	−25.3			
Drilled core (DC1)						
1.2		0	−26.2			
3.5	0.05	0	−26.8			
4.4	0.05	0	−27.3			
6.2		0	−26.8			
10.8	0.03	0	−26.5			
15.3	0.04	0	−26.9			
23.0		1.5	−25.9	−6.1		
24.5		7.8	−27.1	−5.7		
Drilled core (DC3)						
6.5			−27.8	−1.1		
6.5					−2.9	2.9
6.9					−10	0.8
14.5					−11.5	0.7

[a] Data for DC1 core have been previously reported in Jin et al. (2010).
[b] Data for those DC3 core samples have been previously reported in Brantley et al. (2013).
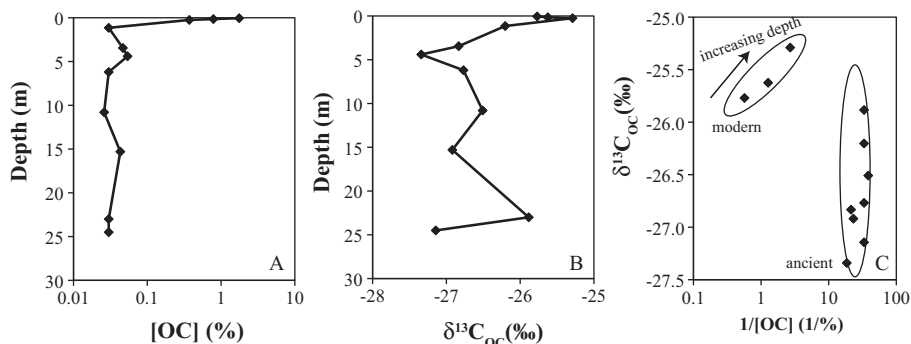
Fig. 2. Organic carbon concentration ([OC] in wt%; A) and its carbon isotope ratio ($\delta^{13}C_{OC}$ in ‰, B) as a function of depth at SSHO. The data shown here are combined profiles from the soils at the SPRT site and drill core samples from the DC1 site. The cross plot of two parameters (C) shows two groups of organic carbon: modern and ancient (from the Silurian bedrock shale).

4.2. Soil gas CO_2 concentrations and $^{13}C_{CO2}$

The CO_2 concentration (pCO_2) and carbon isotopic composition ($\delta^{13}C_{CO2}$) of soil gas samples are reported in Table 2. The soil pCO_2 ranges from 1200 to 30,000 ppmv. The June samples have higher pCO_2 than those from April (Fig. 3A). The highest concentrations are observed at SPVF, SSMS and SSVF sites, where soils are much thicker (>70 cm) (Table 2). In all three sites, soil pCO_2 increases with depth, and even the soil gas samples collected at 10 cm have much higher pCO_2 than atmosphere. This concentration gradient drives CO_2 loss from soils to atmosphere via diffusion. The CO_2 fluxes, which vary among sites, also vary seasonally from 1.1 to 7.3 $\mu mol\,m^{-2}\,s^{-1}$ (Hasenmueller et al., 2014). Indeed, the average surface CO_2 fluxes measured at the SPRT, SPMS and SPVF sites are 3.1, 2.5, and 3.1 $\mu mol\,m^{-2}\,s^{-1}$, respectively (Hasenmueller et al., 2014).

The values of $\delta^{13}C_{CO2}$ in soil gas range from −26.9‰ to −11.7‰. These values are distinctively different from that of atmospheric CO_2 (−8‰) (Fig. 3B). At the SPRT site, where both $\delta^{13}C_{CO2}$ and $\delta^{13}C_{OC}$ were measured, soil gas CO_2 is about 2‰ enriched relative to the soil organic carbon. Near the surface, soil $\delta^{13}C_{CO2}$ values are closer to that of the atmosphere (Fig. 3B). Indeed, shallow soil gas samples, especially those collected from April, have much lower pCO_2, due to mixing with the atmosphere (Fig. 3C).

4.3. Soil water, groundwater and stream chemistry

Elemental and isotope chemistry of soil waters, groundwaters, and stream waters at SSHO are reported in Table 3. The soil waters are dilute, with low Mg^{2+} and Ca^{2+} concentrations (<100 μM) and alkalinity (<200 $\mu eq/L$) (Fig. 4A). Groundwater chemistry varies among sites, but is generally more concentrated than soil waters (Fig. 4A). The highest Mg^{2+}, Ca^{2+} and alkalinity concentrations are observed in the wells near the outlet of the catchment (wells #17, #18, #2, and #3), and the lowest concentrations are observed higher in the catchment (wells #10, #11) (Table 3). Stream Mg^{2+} and Ca^{2+} concentrations increase downstream from SH to SM and SW (Fig. 4A; Table 3). Strontium behaves similarly to Ca and Mg, and follows their concentration trends (Table 3). Dissolved Fe and Mn concentrations are

low in these groundwaters (<2 μM), except in well #8 (>20 μM) (Table 3).

Soil waters have lower pH (4–5.5) than groundwaters (5.5–7.5), and stream pH lies between (Fig. 4B). The pH of the stream becomes higher moving downstream from the headwater to outlet (Table 3). The pH of the stream at each location varies among the three sampling trips, possibly due to the relative contributions from groundwater and soil water, and due to the in-situ biological activities. All the water samples are unsaturated with respect to calcite and disordered dolomite, with negative saturation indices (Table 3; Fig. 4B). The soil waters are the farthest from equilibrium (Fig. 4B). The saturation indices of the groundwaters with respect to calcite vary among sites, and those near the outlet are close to 0 (Table 3), in agreement with trends of Ca, Mg and alkalinity concentrations as well as pH values. The saturation indices for calcite in the stream waters are intermediate, and slightly overlap with groundwaters (Fig. 4B).

The $\delta^{13}C_{DIC}$ values range from −22‰ to −17‰ in soil waters, from −18.4‰ to −9.9‰ in groundwaters, and from −17.9‰ to −10.6‰ in streams (Table 3, Fig. 4C). Well #8 was documented to have much higher $\delta^{13}C_{DIC}$ values: −3.1‰ in November 2011 and −0.9‰ in April 2012. The $\delta^{13}C_{DIC}$ values increase systematically downstream from values similar to soil waters to that of ground waters (SH: −19.9‰ and −17.4‰; SM: −15.8‰ and −15.9‰; and SW: −12.6‰ and −10.6‰, for November 2011 and April 2012, respectively) (Table 3).

The SO_4^{2-} concentrations in soil waters vary from 25 to 150 μM, while most groundwaters have SO_4^{2-} concentrations higher than 80 μM, except for wells #8 and #18. In contrast, SO_4^{2-} concentrations vary little in the stream (Table 3). The $\delta^{34}S_{SO4}$ values of the stream also remain constant at ∼ 3‰; however, groundwaters have a wider range of $\delta^{34}S_{SO4}$ values (Table 3).

5. DISCUSSION

The SSHO catchment provides a natural laboratory to investigate C transformations during shale weathering in a watershed of relatively simple lithology and hydrology. This case study constrained shale's potential to consume CO_2, by weathering of silicate minerals in shallow soils and by dissolution of trace carbonate minerals deep in

Table 2
CO$_2$ concentrations and isotope compositions of soil gas.

Collection date	Site	Depth cm	pCO$_2$ ppm	$\delta^{13}C_{CO2}$ ‰
6/6/2012	SPRT	20	3960	−23.4
6/6/2012	SPMS	10	2328	−26.9
6/6/2012	SPMS	20	2986	−24.0
6/6/2012	SPMS	40	3225	−23.8
6/6/2012	SPVF	10	1222	−21.8
6/6/2012	SPVF	30	3813	−23.1
6/6/2012	SPVF	50	5812	−23.6
6/6/2012	SPVF	70	16627	−23.9
4/15/2013	SPMS	10	1232	−11.7
4/15/2013	SPMS	20	1485	−16.2
4/15/2013	SPMS	40	1428	−17.1
4/15/2013	SPVF	10	1315	−15.2
4/15/2013	SPVF	30	4707	−20.8
4/15/2013	SPVF	50	5591	−21.3
6/6/2012	SSRT	10	1260	−21.4
6/6/2012	SSRT	30	7127	−23.6
6/6/2012	SSMS	10	4681	n.a.
6/6/2012	SSMS	20	17170	−25.4
6/6/2012	SSMS	40	20886	−24.4
6/6/2012	SSMS	60	17786	−24.0
6/6/2012	SSMS	80	24874	−24.2
6/6/2012	SSMS	100	29549	−23.7
6/6/2012	SSMS	130	21949	−24.0
6/6/2012	SSMS	160	24487	−23.9
6/6/2012	SSVF	10	2899	−23.1
6/6/2012	SSVF	30	12823	−25.1
6/6/2012	SSVF	50	12719	−26.1
6/6/2012	SSVF	70	15793	−25.7
6/6/2012	SSVF	90	10269	−26.3
4/15/2013	SSRT	20	2279	−19.2
4/15/2013	SSRT	30	3078	n.a.
4/15/2013	SSMS	10	1943	−18.2
4/15/2013	SSMS	20	5656	−20.7
4/15/2013	SSMS	40	7182	−20.8
4/15/2013	SSMS	60	5760	−20.6
4/15/2013	SSMS	80	7759	−21.7
4/15/2013	SSMS	100	9193	−22.0
4/15/2013	SSMS	130	6719	−22.0
4/15/2013	SSMS	160	8296	−22.1
4/15/2013	SSVF	10	1701	−18.0
4/15/2013	SSVF	30	4258	−23.0
4/15/2013	SSVF	50	4032	−22.3
4/15/2013	SSVF	70	5394	−22.1
4/15/2013	SSVF	90	4281	−23.0

n.a. = not available, due to broken sample vial.

saprock and bedrock. Below, we will focus our discussion on the decomposition of ancient and modern organic matter, production rates of soil CO$_2$, and C sources of DIC in soil water, groundwater and stream samples. In addition, we will determine the relative importance of carbonic versus sulfuric acid weathering pathways during shale alteration.

5.1. Contribution of ancient versus modern organic matter to soil CO$_2$

The release rate of Silurian organic carbon can be estimated using a simple mass-balance calculation as discussed below. The amount of OC present in a unit volume of bedrock is calculated as:

$$M_{OC} = [OC] * \rho_P / MW_C = 63 \text{ mol m}^{-3} \qquad (1)$$

Here [OC] is organic carbon content of parent (0.03 wt%), ρ_P is bulk density of parent shale (2.5 g cm^{-3}), and MWc is molecular weight of carbon (12 g mol^{-1}) (Table 4). The rate of soil production (P), i.e., the conversion rate for saprock to soil, is approximately 20 mM yr^{-1} as measured for the ridge top of SSHO (Ma et al., 2011, 2014). Assuming that depletion of organic matter is fast after being exposed, then the depletion rate of ancient OC (F$_{OC}$) at the ridge top can be calculated as:

$$F_{OC} = M_{OC} * P = 1.3 \text{ mol m}^{-2} \text{ kyr}^{-1} \qquad (2)$$

The CO$_2$ efflux (from soil to atmosphere) measured with flux chambers between 2009 and 2011 is ~ 1 μmol m^{-2} s^{-1}, or 3×10^4 mol m^{-2} kyr^{-1}. This CO$_2$ efflux is averaged from monthly measurement along a planar transect and a swale transect, and thus it is reasonable to consider this rate to be representative for the whole catchment (Hasenmueller et al., 2014). The modern soil respiration is thus more than four orders of magnitude higher than F$_{OC}$. This discrepancy is consistent with the inference that soil gas CO$_2$ is almost entirely derived from root respiration, microbial respiration and oxidation of modern OC. The contribution from respiration of ancient organic matter is negligible.

The soils have $\delta^{13}C_{OC}$ values of ~ -27‰, consistent with the C$_3$ type forest coverage (Hillaire-Marcel, 1986; Ehleringer et al., 1991; Vogel, 1993). Within the ridgetop site, $\delta^{13}C_{OC}$ values increased with depth (Table 2: Fig. 2B). A similar depth trend has been commonly observed elsewhere and may be related to preferential release of ^{12}C during decomposition (Koutika et al., 1997; Trumbore, 2000; Wynn et al., 2005; Amiotte-Suchet et al., 2007; Boström et al., 2007). The organic matter in deep DC1 core samples (representative of parent Rose Hill shale) was measured to have $\delta^{13}C_{OC}$ values around -27‰, falling within the range of marine organic matter of Silurian age (Kump and Arthur, 1999). This signature cannot be distinguished isotopically from modern vegetation.

The $\delta^{13}C_{CO2}$ values are higher than that of soil organic matter (Table 1; Table 2), and similar trends have been observed in other soils worldwide (Cerling et al., 1991; Jin et al., 2011). Such isotopic fractionation is attributed to diffusional loss of CO$_2$ out of the soil at the land surface due to the concentration gradient, as soil respiration discriminates C isotopes insignificantly (Cerling et al., 1991; Ekblad et al., 2002; Boström et al., 2007). Indeed, a typical diffusion curve is observed at SSHO, with pCO$_2$ decreasing upward (Fig. 3A). This kinetic process enriches the soil gas CO$_2$ in ^{13}C by a maximum of about 4.4‰ relative to respired CO$_2$ (Cerling et al., 1991). Thus, the $\delta^{13}C_{CO2}$ near the soil surface deviates from the $\delta^{13}C_{OC}$ in the soil by more than 4.4‰, as expected.

5.2. Changes in DIC concentration and $\delta^{13}C_{DIC}$ from soil water to groundwater

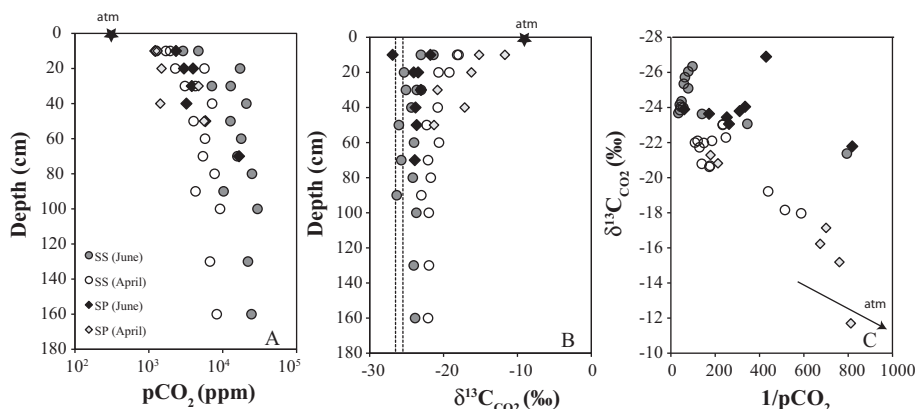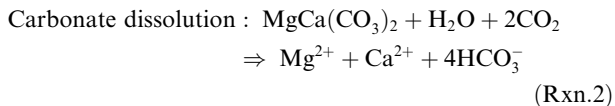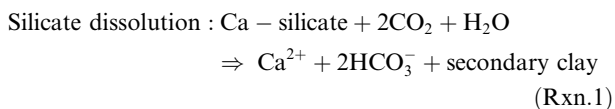Previous carbon isotope studies have mainly focused on riverine waters, with little information available for soil

Fig. 3. Soil gas CO_2 concentrations (pCO_2 in ppmv; A) and its carbon isotope ratio ($\delta^{13}C_{CO2}$ in ‰; B) as a function of depth for the ridge top (SSRT, SPRT), mid-slope (SSMS, SPMS) and valley floor (SSVF, SPVF) locations. Atmospheric pCO_2 and $\delta^{13}C_{CO2}$ are plotted for comparison as stars. The SPRT soil CO_2 is slightly enriched in ^{13}C relative to its soil organic carbon source (dashed lines delineate the range in values). Correlation between pCO_2 and $\delta^{13}C_{CO2}$ documents the mixing curve between soil and atmospheric CO_2 (arrow).

waters even though this is a critical zone of carbon transformation (Brunet et al., 2005; Jin et al., 2009). The weathering sequences at SSHO are closely linked to carbon cycles (Jin et al., 2010; Brantley et al., 2013), as silicate and carbonate dissolution each have a different capacity to consume CO_2:

Silicate dissolution : $Ca - silicate + 2CO_2 + H_2O$
$$\Rightarrow Ca^{2+} + 2HCO_3^- + secondary\ clay$$
(Rxn.1)

Carbonate dissolution : $MgCa(CO_3)_2 + H_2O + 2CO_2$
$$\Rightarrow Mg^{2+} + Ca^{2+} + 4HCO_3^-$$
(Rxn.2)

Before the CO_2 consumption extents can be quantified, the atmospheric contribution needs to be evaluated. To do so, monthly rainfall chemistry data (2010–2013) from two nearby National Atmospheric Deposition Program (NADP) sites (PA15 and PA42) near SSHO were downloaded. The Ca and Mg concentrations in the snow or rain varied among different months (Ca: 0.8–8.4 µM; Mg: 0.33–2.2 µM) and averaged 3.0 µM and 0.86 µM, respectively. Given that half of the precipitation is lost through evapotranspiration (Jin et al., 2011), the remaining Ca and Mg in water that infiltrates to the deeper soils and underlying rock is thus doubled in concentration (6.0 and 1.7 µM, respectively). However these values are still much lower than those observed in soil water, stream water and groundwater samples. Thus the contribution from precipitation to the overall elemental budget is negligible for Ca and Mg but still is corrected as discussed below. The average sulfate concentration in the wet precipitation is 11 µM for 2011–2013.

A variable amount of ankerite is present in the Rose Hill bedrock, but it is depleted in the soils and the saprock (Jin et al., 2010; Brantley et al., 2013). Thus, the soil water is controlled by silicate dissolution (with a negligible contribution from wet precipitation). This is in agreement with the low concentrations of Ca^{2+}, Mg^{2+} and alkalinity observed (Fig. 4A; Jin et al., 2011). Here, the only C source in soil water DIC is soil CO_2 (Rxn. (1)). If the soil water is

in contact with soil CO_2 for a long time, then all DIC species (i.e., H_2CO_3, HCO_3^- and CO_3^{2-}) will reach isotopic equilibrium with soil CO_2 with fractionation factors dictated by the soil water temperature (Mook et al., 1974). Given that the speciation of DIC (i.e., the relative abundance of the three carbonate species) depends on pH and temperature, the overall difference between $\delta^{13}C_{DIC}$ and $\delta^{13}C_{CO2}$ is also governed by pH and temperature. We modeled such relationships using measured parameters (pH, $\delta^{13}C_{CO2}$) and fractionation factors in the literature (Mook et al., 1974). The mean annual air temperature of 10 °C was used for all calculations reported below. Calculations based on 5 and 15 °C revealed that neither the isotope fractionation factors nor the $\delta^{13}C_{DIC}$ values were greatly affected by variations in temperature. Isotopic equilibrium between soil CO_2 and soil water DIC is expected (Jin et al., 2009) because: (1) the soil gas is a relatively large C reservoir while the consumption of CO_2 by silicate dissolution is small; and (2) soil water stays in the soil profile for days (Jin et al., 2011), providing sufficient time to reach isotopic equilibrium with soil CO_2.

If the DIC in natural waters does not attain isotopic equilibrium with soil CO_2, for example, in a closed system, then $\delta^{13}C_{DIC}$ is controlled by the isotopic composition of its carbon sources. In the case of silicate weathering with soil CO_2, the $\delta^{13}C_{DIC}$ equals $\delta^{13}C_{CO2}$. In the case of carbonate weathering with CO_2 (Rxn. (2)), the $\delta^{13}C_{DIC}$ equals ½($\delta^{13}C_{CO2} + \delta^{13}C_{CaCO3}$), i.e., ~-14‰ in our system using measured parameters ($\delta^{13}C_{CO2} = -22$‰; $\delta^{13}C_{CaCO3} = -6$‰). At the higher pH of the groundwaters, the values associated with equilibration with soil $\delta^{13}C_{CO2}$ and with mixing with $\delta^{13}C_{DIC}$ are similar, and thus C isotopic composition alone cannot be used to determine if the system is closed to CO_2.

Even so, we assume that groundwaters that have much higher DIC concentrations have C isotope ratios controlled not by soil CO_2 but rather by mixing with deeper waters that have dissolved carbonates. This inference is defensible because CO_2 transport is limited by diffusion and groundwater is too deep to be connected with soil CO_2. Furthermore,

Table 3
Chemistry and isotope composition of soil water, groundwater and stream water samples.

Sample	Depth cm	Sampling date	Temp °C	pH	Conductivity µs/cm	$\delta^{13}C_{DIC}$ ‰	$\delta^{34}S$ ‰	Alkalinity µeq/L	Cl^- µM	NO_3^- µM	SO_4^{2-} µM	Al µM	Ca^{2+} µM	Fe µM	K^+ µM	Mg^{2+} µM	Mn µM	Na^+ µM	H_4SiO_4 µM	Sr^{2+} µM	Alk[1] µeq/L	pCO_2[2] Bar	Calcite[2] Log SI	Dolomite[2] Log SI
Well																								
#10		11/6/2011		5.26		−16.3			40	30.2	121	0.4	94	0.2	32	103	0.3	40	116	0.2	151	0.049	−4.7	−8.3
#11		11/6/2011		5.80		−15.2			23	7.1	91	8.5	95	2.4	23	114	0.0	45	133	0.2	269	0.024	−3.9	−6.7
#17		11/6/2011		6.58		−9.9			55	17.1	117	BD	1236	BD	18	225	0.0	58	104	1.0	2686	0.039	−1.1	−1.9
#18		11/6/2011		6.61		−11.6			51	29.7	55	38.3	759	9.6	73	172	1.3	500	243	0.7	2237	0.030	−1.3	−2.3
#4		11/6/2011		6.53		−11.5			48	46.7	120	0.7	324	0.2	32	198	0.2	71	101	0.8	807	0.014	−2.2	−3.5
#5		11/6/2011		5.70		−17.3			21	2.1	78	1.0	101	0.2	23	68	BD	19	100	0.1	199	0.023	−4.1	−7.3
#6		11/6/2011		6.40		−13.1			24	3.5	107	0.9	452	0.1	24	289	BD	175	111	1.0	1436	0.033	−1.9	−3.0
#8		11/6/2011		6.48		−3.1			36	41.4	44	0.7	424	13.9	62	329	45.0	86	113	0.5	1482	0.028	−1.8	−2.8
#10		5/1/2012		5.86		−17.7	1.8	203	24	2.1	125	2.3	72	0.1	27	88	BD	28	170	0.1		0.016	−4.1	−7.0
#11		5/1/2012		6.04		−18.0	3.1	330	22	8.3	90	3.8	88	6.2	20	106	0.2	21	179	0.2		0.017	−3.6	−8.8
#17		5/1/2012		7.42		−10.7	0.6	1941	51	2.6	114	1.7	1104	0.1	10	218	1.4	43	140	1.0		0.011	−0.8	−1.3
#18		5/1/2012		6.70				625	149	16.5	26													
#4		5/1/2012		7.39		−10.6	−9.6	1401	26	8.4	144	1.9	580	0.1	22	355	BD	82	142	1.6		0.003	−0.8	−0.9
#5		5/1/2012		5.85		−18.4	4.0	215	18	5.7	80	2.3	89	0.1	21	67	0.1	11	134	0.1		0.017	−3.9	−7.0
#6		5/1/2012		7.35		−13.3	−7.7	1215	18	5.3	108	2.4	422	0.3	29	266	0.3	142	145	0.9		0.003	−1.1	−1.3
#8		5/1/2012		6.49		−0.9	6.5	2000	20	0.2	13	2.4	387	34.3	44	297	50.5	59	191	0.5		0.037	−1.8	−2.6
#2		4/13/2013	9.4	7.40	264.0	−13.1	1.6		37	1.3	130	8.4	1333	4.3	19	120	0.7	40	143	0.8	2665	0.006	−0.3	−2.3
#3		4/13/2013	7.2	6.65	164.0	−16.4	3.8		35	0.4	147	46.1	805	16.8	19	78	2.1	37	209	0.6	1493	0.017	−1.6	−4.8
#4		4/13/2013	6.8	7.24	160.0	−13.5	−2.0		23	2.0	135	BD	345	BD	19	216	0.3	55	116	1.0	899	0.003	−1.5	−3.9
#5		4/13/2013	8.2	6.05	45.8	−20.9	4.5		15	0.4	81	7.8	111	4.5	24	70	2.4	16	127	0.1	224	0.011	−3.8	−8.4
#6		4/13/2013	7.9	7.26	215.0	−13.2	−14.9		21	0.3	150	1.5	684	1.3	22	415	0.4	252	142	1.7	2152	0.007	−0.8	−2.6
#8		4/13/2013	8.3	6.58	118.0	−14.1	6.5		36	2.9	98	2.9	141	14.7	54	156	18.7	58	140	0.3	472	0.007	−2.8	−6.2
#10		4/13/2013	8.2	6.30	41.2	−21.8	3.9		18	1.9	109	11.8	64	6.5	29	84	0.7	25	157	0.2	112	0.003	−4.1	−8.8
#11		4/13/2013	7.9	6.22	50.6	−19.4	3.9		20	7.5	95	1.4	84	0.8	22	107	0.3	36	157	0.2	225	0.008	−3.7	−8.0
#17		4/13/2013	7.7	7.52	266.8	−12.1	−0.1		49	0.1	114	BD	1122	0.1	13	207	0.2	38	126	1.0	2433	0.004	−0.3	−2.1
Stream																								
SH		11/18/2011		4.62		−17.9			21	2.4	86	0.8	57	0.1	24	78	0.1	23	88	0.1	120			
SM		11/18/2011		5.09		−15.8			25	1.9	93	1.1	100	0.1	24	90	BD	32	93	0.2	218			
SW		11/18/2011		5.25		−12.6			22	0.0	91	0.8	126	0.1	22	96	BD	30	93	0.2	287			
SH		5/1/2012		6.04		−17.4	3.9	142	19	5.6	92	2.3	58	0.1	23	79	BD	20	136	0.1		0.007	−4.1	−7.1
SM		5/1/2012		6.22		−15.9	4.0	198	18	6.6	93	2.4	55	0.3	20	80	BD	16	137	0.1		0.007	−3.8	−6.4
SW		5/1/2012		6.85		−10.6	3.1	351	20	2.7	97	2.4	169	0.3	21	94	0.1	26	137	0.3		0.003	−2.5	−4.2
SH		4/13/2013	7.6	6.05	31.5	−21.1	4.4		16	2.5	88	1.0	46	0.9	23	65	0.8	11	103	0.1	62	0.003	−4.7	−9.9
SM		4/13/2013	7.8	6.52	32.7	−19.3	3.5		16	2.7	90	BD	47	BD	22	68	BD	14	109	0.1	67	0.001	−4.2	−8.8
SW		4/13/2013	8.5	7.10	42.0	−16.3	3.6		17	1.6	91	0.1	90	0.1	21	71	BD	16	112	0.2	158	0.001	−2.9	−6.1

Table 3 (continued)

Sample	Depth cm	Sampling date	Temp °C	pH	Conductivity μs/cm	δ13C$_{DIC}$ ‰	δ34S ‰	Alkalinity μeq/L	Cl⁻ μM	NO₃⁻ μM	SO₄²⁻ μM	Al μM	Ca²⁺ μM	Fe μM	K⁺ μM	Mg²⁺ μM	Mn μM	Na⁺ μM	H₄SiO₄ μM	Sr²⁺ μM	Alk[1] μeq/L	pCO₂[2] Bar	Calcite[2] Log SI	Dolomite[2] Log SI
Soil water																								
SPVF	10	11/18/2011		4.77		−19.1			39	3.1	100	8.4	63	0.5	16	33	0.1	22	99	0.2	−13			
SPVF	20	11/18/2011		4.68		−19.4			57	BD	73	8.0	60	0.9	16	42	0.2	23	87	0.2	32			
SPVF	30	11/18/2011		4.90		−20.2			34	2.9	118	11.5	90	0.4	17	55	0.3	31	140	0.3	63			
SPVF	40	11/18/2011		5.20		−18.9			34	1.2	68	1.8	66	0.1	18	61	0.2	32	88	0.2	131			
SPVF	60	11/18/2011		5.33					35	11.4	94	3.5	86	0.9	22	86	0.3	35	98	0.3	163			
SPMS	10	11/18/2011		4.71					7	0.6	54	3.1	18	0.2	9	32	0.7	15	89	0.1	6			
SPMS	40	11/18/2011		4.35		−17.1			28	1.8	104	4.2	58	0.1	9	74	0.3	25	127	0.2	56			
SPMS	50	11/18/2011		4.72		−19.7			20	BD	134	1.6	54	0.3	10	50	0.9	24	93	0.2	−49			
SPRT	10	11/18/2011		4.47		−19.7			31	BD	79	18.5	54	1.1	26	32	2.1	22	85	0.2	28			
SPRT	20	11/18/2011		4.33		−18.1			15	2.7	60	5.0	42	0.3	12	21	0.8	18	71	0.2	15			
SPRT	30	11/18/2011		4.49					15	BD	62	2.6	59	0.1	9	20	0.2	23	84	0.2	46			
SPVF	20	5/1/2012		5.46				85.9	16	3.6	68	6.6	47	0.3	14	34	0.1	10	124	0.1		0.016	−5.0	−9.2
SPVF	30	5/1/2012		5.18		−21.8			15	5.7	133	12.0	88	0.4	14	58	0.2	27	270	0.3				
SPVF	40	5/1/2012		5.61		−21.0		165	30	3.5	94	3.4	59	0.1	18	56	0.1	28	125	0.2		0.023	−4.5	−8.0
SPVF	60	5/1/2012				−17.1			22	2.2	88	2.5	66	0.1	14	71	BD	4	147	0.2				
SPMS	40	5/1/2012		5.15				83	9	0.7	107	4.5	42	0.1	6	56	0.2	7	181	0.1		0.034	−5.4	−9.6
SPRT	20	5/1/2012		5.34		−19.2			16	0.4	53	5.2	37	0.1	8	21	0.2	1	107	0.1				
SPRT	30	5/1/2012		5.46		−19.6			22	3.9	61	4.4	45	0.1	5	21	0.1	BD	120	0.2				
SPRT	10	4/15/2013	10.3	4.99		−21.7			25	0.8	33	9.6	28	0.6	23	14	1.0	16	85	0.1	32	0.002	−6.2	−13.4
SPRT	20	4/15/2013	10.7	5.04					49	5.7	54	1.3	28	BD	12	16	0.2	12	102	0.1	−51			
SPRT	30	4/15/2013	10.4	5.04		−22.1			44	2.0	63	3.6	41	0.3	20	21	1.6	21	101	0.1	−8			
SPMS	40	4/15/2013	10.8	5.03					43	18.4	106	1.8	39	0.1	6	54	0.2	16	198	0.1	−65			
SPMS	50	4/15/2013	10.8	5.18					49	11.3	117	11.5	43	2.1	38	40	2.2	25	133	0.1	−65			
SPVF	20	4/15/2013	9.8	5.17					22	3.6	70	4.8	46	0.2	16	34	0.1	12	128	0.2	23	0.008	−6.0	−12.8
SPVF	30	4/15/2013	9.8	4.97					18	1.0	91	12.5	71	0.2	12	43	0.2	14	214	0.2	53	0.031	−5.6	−12.1
SPVF	40	4/15/2013	9.6	5.27					22	0.7	92	1.5	55	BD	13	51	BD	16	125	0.2	34	0.010	−5.6	−11.9
SPVF	60	4/15/2013	10.6	5.66					139	BD	88	0.1	61	3.7	14	67	BD	19	110	0.2	-27			

[1] Alkalinity was calculated based on charge balance.
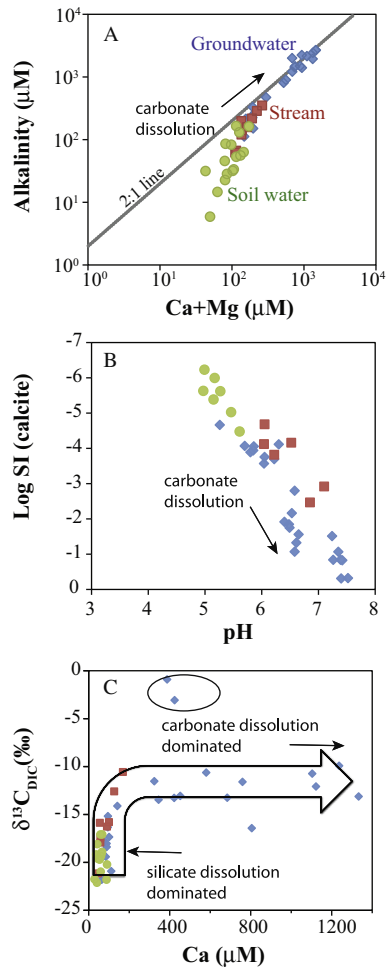[2] Saturation indexes and pCO₂ were calculated using geochemical models. See text for details.

Fig. 4. Plot showing the correlation between divalent cations ($Mg^{2+} + Ca^{2+}$) and alkalinity (A). This correlation demonstrates the evolution of natural waters (soil water, groundwater, and stream water) with progress of chemical weathering. The transition from silicate-dissolution dominated (in soil waters) to carbonate-dissolution dominated (in groundwaters) conditions, is accompanied by increases in pH and saturation indices as the water moves toward equilibrium with carbonates (B). The C isotope composition of DIC ($\delta^{13}C_{DIC}$) changes with Ca^{2+} concentrations in these natural waters, as the system progresses from waters dominated by silicate dissolution to those dominated by carbonate dissolution (C). Well #8 is an outlier in this diagram indicating different controls on its chemistry and C isotope composition as described in the text.

the dissolution rate of ankerite might be much higher than the rate of replenishment of soil CO_2-charged water to the water table. Previous work using an optical televiewer showed that the Rose Hill bedrock at SSHO is fractured (Kuntz et al., 2011) especially in the upper ~5–7 m. This surficial fracturing has been attributed to frost-relating fracturing during glacial periods (Jin et al., 2010). Residence times for groundwaters in this surficial fractured zone are likely less than 1 year, as roughly estimated by water isotopes (Jin et al., 2011; Thomas et al., 2013). Furthermore, below the water table, the diffusion of CO_2 is probably slow (Jahne et al.,

1987), so that ankerite dissolution occurs in a system closed to CO_2.

If so, Ca^{2+} and $\delta^{13}C_{DIC}$ can help identify the dominance of silicate and carbonate dissolution in natural waters (Fig. 4C): soil waters and some groundwaters are influenced only by silicate dissolution while other groundwaters, are influenced by carbonate weathering (except for the one anomalous well, #8). These observations lead to the inference that carbonate dissolution controls groundwater chemistry near or below the water table (Fig. 4A and B).

Groundwater from well #8 has elemental chemistry and pH values similar to other groundwater samples, except for extremely elevated dissolved Fe and Mn concentrations and low SO_4^{2-} concentrations. Ankerite has significant Fe and Mn in its dolomite-like structure, and thus Fe and Mn are released during ankerite dissolution. For most of the wells, the groundwaters probably remain oxic, leading to Fe and Mn precipitation immediately after dissolution. Monitoring of water isotopes has revealed almost constant $\delta^{18}O$ and δ^2H values for deep wells (>3 m) (Jin et al., 2011; Thomas et al., 2013), indicative of a longer residence time and thus deep sources of groundwater. It is therefore likely that samples from well #8 are O_2-depleted. This reducing condition in well #8 allows elevated dissolved Fe and Mn, which are otherwise insoluble in oxic environments. These groundwater samples from well #8 are also characterized by higher $\delta^{13}C_{DIC}$ values, deviated from the mixing lines defined by silicate and carbonate dissolution (Fig. 4C). This probably suggests that carbon reduction (methanogenesis) might be occurring, producing methane with extremely negative $\delta^{13}C_{DIC}$, leaving residual DIC that is enriched in ^{13}C. These arguments could be consistent with the conclusion that groundwaters from well #8 are from a much deeper source than are accessed by the other boreholes that allow access only to shallow groundwater systems. The groundwater from well #8 could flow up through fractures from deep bedrock. Future work is needed to constrain this C transformation process.

5.3. Other acidity involved in chemical weathering

Besides CO_2, other sources of acidity are also involved in chemical dissolution reactions at the SSHO. Indeed, dissolved organic carbon (DOC) concentrations of soil waters are high in shallow soils and decrease with depth (Andrews et al., 2011; Jin et al., 2011). In addition, the wet precipitation and biological processes contribute to nitric acids in the shallow soils. Thus organic and nitric acids are expected to be important in shallow soils, where only silicate minerals dissolve. In this case, these organic and inorganic acids impact DIC and $\delta^{13}C_{DIC}$ by modifying the pH. DOC is consumed by micro-organisms to release CO_2; however, CO_2 will not likely directly alter $\delta^{13}C_{DIC}$ values. Acids involved in silicate versus carbonate weathering in different locations are presented in Fig. 5A.

At more than 20 m depth, the pyrite-weathering front is observed near the ankerite weathering front, and both are within meters of the water table (Brantley et al., 2013). Oxidative dissolution of pyrite releases sulfuric acid and

Table 4
Parameters and their values used for CO_2 flux calculation.

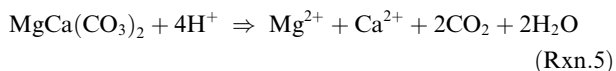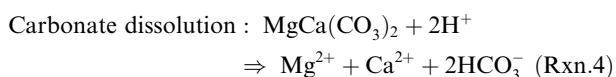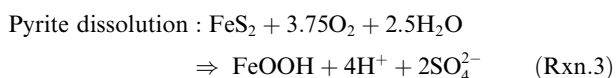| Parameters	Symbol	Values	Units
Parent organic carbon concentration	$[OC]$	0.03	wt%
Molecular weight for carbon	MW_C	12	g mol^{-1}
Parent ankerite concentration	$C_{ankerite}$	7.8	wt%
Molecular weight for dolomite (estimate for ankerite)	$MW_{ankerite}$	184	g mol^{-1}
Soil production rate[a]	P	20	mM yr^{-1}
Parent bulk density	ρ_P	2.5	g cm^{-3}
Mean annual precipitation	MAP	107	cm yr^{-1}
Discharge from the catchment	$D = 1/2$MAP	53.5	cm yr^{-1}
Ca concentration in the rain	$[Ca^{2+}]_{ppn}$	3	μmol L^{-1}
Mg concentration in the rain	$[Mg^{2+}]_{ppn}$	0.9	μmol L^{-1}
Ca concentration in soil water	$[Ca^{2+}]_{SoilWater}$	55	μmol L^{-1}
Mg concentration in soil water	$[Mg^{2+}]_{SoilWater}$	48	μmol L^{-1}
Ca concentration in the stream	$[Ca^{2+}]_{stream}$	108	μmol L^{-1}
Mg concentration in the stream	$[Mg^{2+}]_{stream}$	86	μmol L^{-1}
Average soil CO_2 concentrations	pCO_2	40000	ppmv
Henry's Law constant for CO^2 at 10 °C	K_{CO_2}	$10^{-1.47}$	
CO_2 fluxes from soils to groundwater, controlled by equilibrium with pCO_2	F_{H2CO3}^{*}	72	mol m^{-2} kyr^{-1}
CO_2 release rate by OM oxidation	F_{OC}	1.3	mol m^{-2} kyr^{-1}
CO_2 consumption rate by silicate dissolution (short-term)	$F_{silicate}$	44	mol m^{-2} kyr^{-1}
CO_2 consumption rate by ankerite dissolution (long-term)	$F_{ankerite}$	42	mol m^{-2} kyr^{-1}
CO_2 consumption rate by ankerite dissolution (short-term)	$F_{ankerite}$	48	mol m^{-2} kyr^{-1}

[a] From Ma et al. (2010).
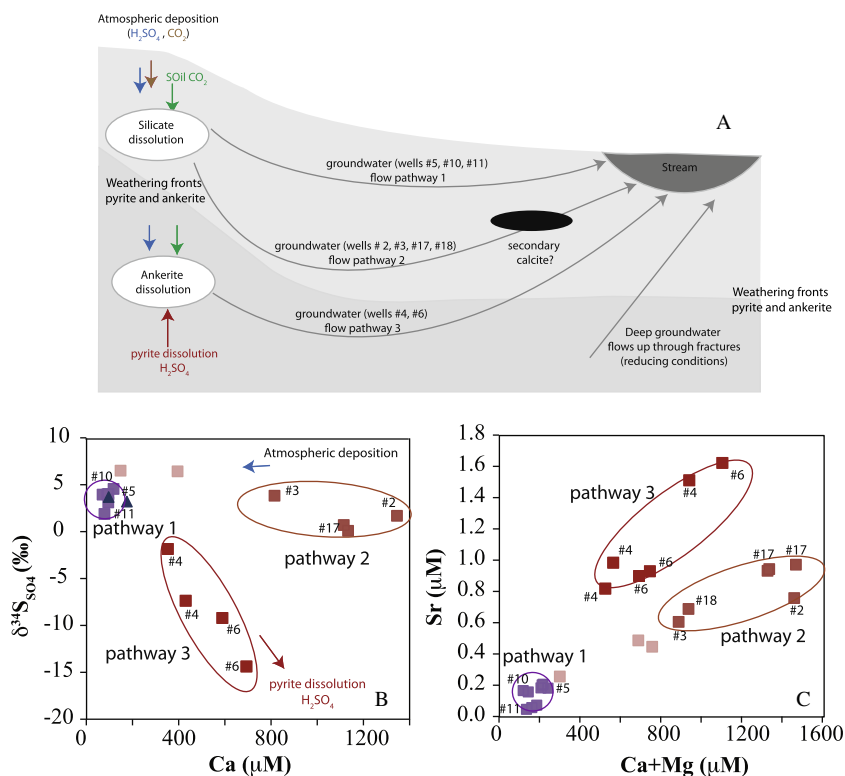
Fig. 5. A conceptual model illustrating the locations of silicate and carbonate dissolution and the sources of acidity involved in these reactions (A). Three flow pathways are hypothesized to explain three types of groundwater (1: silicate dissolution driven by precipitation-derived protons; 2: secondary carbonate dissolution driven by precipitation-derived protons; and 3: primary carbonate (ankerite) dissolution driven by pyrite-dissolution). As the mineral–water interfacial area per unit volume decreases downward (due to increasing grain size and decreasing fracture spacing), solute transport in groundwater can be conceptualized as dominated by advection with diffusion into rock matrix as a minor contributor in shallow layers, to advection with diffusion into rock matrix as a major contributor in deeper layers. The systematics of sulfur at the SSHO (B) and Sr^{2+} vs. $Ca^{2+} + Mg^{2+}$ (C) clearly show the three types of groundwater (squares), corresponding to the three flow pathways in (A). The $\delta^{34}S_{SO4}$ of streams at the outlet (triangles) indicates that wet deposition is the dominant source of SO_4^{2-}.

thus helps dissolve the carbonate mineral, ankerite (Rxns. ((3)–(5))).

Pyrite dissolution : $FeS_2 + 3.75O_2 + 2.5H_2O$
$$\Rightarrow FeOOH + 4H^+ + 2SO_4^{2-} \quad (Rxn.3)$$

Carbonate dissolution : $MgCa(CO_3)_2 + 2H^+$
$$\Rightarrow Mg^{2+} + Ca^{2+} + 2HCO_3^- \quad (Rxn.4)$$

$$MgCa(CO_3)_2 + 4H^+ \Rightarrow Mg^{2+} + Ca^{2+} + 2CO_2 + 2H_2O \quad (Rxn.5)$$

Depending on the molar ratio of H^+ and carbonate, either HCO_3^- or CO_2 could be formed (Rxn. (4) or Rxn. (5)), impacting the C speciation and its isotope ratios differently. Li et al. (2008) observed a positive correlation between SO_4^{2-}/DIC and riverine $\delta^{13}C_{DIC}$ in southwest China as sulfuric acid of an atmospheric origin reacted with carbonate as opposed to carbonic acid. Similarly, weathering of sulfide minerals is shown to be as important as carbonic acid in the McKenzie River Basin (Calmels et al., 2007; Beaulieu et al., 2011). Also, in volcanic Caribbean islands, magmatically-derived CO_2, H_2S and SO_2 lead to fast volcanic rock weathering where magmatic CO_2 contributes up to 60% of riverine DIC (Rive et al., 2013).

C isotope systematics during carbonate dissolution by strong acids can be quantitatively evaluated using SO_4^{2-}/DIC equivalent ratios. Indeed, the SO_4^{2-}/DIC ratio is 0 if neither Rxn. (3) nor Rxn. (4) occurs in carbonic acid-dominate scenarios. The ratio is 1 if Rxn. (2) does not occur in sulfuric acid-dominated scenarios. At the SSHO, only trace amounts of pyrite are present, versus ∼7.8 wt% of ankerite observed in the Rose Hill bedrock (Jin et al., 2010). Indeed, Brantley et al. (2013) defined the acid-generating capacity R (the molar ratio of pyrite to calcite in parent materials) to be much smaller than 1, and suggested that sulfuric acid is completely consumed during carbonate dissolution. Thus it is reasonable to assume that Rxn. (5) is insignificant. To summarize, for carbonate weathering, Rxn. (2) dominates with some influence from Rxn. (4). Thus, C in DIC is sourced from both CO_2 and $CaCO_3$, but their relative contribution is not 1:1. Instead, more C is from $CaCO_3$ than from CO_2 and thus $\delta^{13}C_{DIC}$ values of groundwaters that have been impacted by carbonate dissolution are closer to that of the $CaCO_3$ end-member (Fig. 4C).

At the SSHO, aqueous SO_4^{2-} is derived from pyrite dissolution and wet deposition (Fig. 5A). Specifically, this part of central Pennsylvania has been highly impacted by acid rain (Wadleigh et al., 1994; Alewell et al., 2000), making it impossible to model the $\delta^{13}C_{DIC}$ of groundwaters in great detail. Nonetheless, it is defensible to assume that DIC was derived in a 1:1 ratio from CO_2 and ankerite. As pyrite is largely absent from the soils, we assume that soil water SO_4^{2-} is entirely from wet deposition (both modern and ancient). The SO_4^{2-} concentrations show more complex variation with depth and also landscape position, probably related to S cycling within soil profiles.

The source of SO_4^{2-} in the pyrite-free zone is confirmed by S isotope ratios. Although the S isotopes in soil water were not measured due to insufficient volume of samples, SO_4^{2-} in some groundwaters has $\delta^{34}S_{SO4}$ values between 0‰ and 8‰ (Fig. 5B), well within the range of acid deposition observed for this region (Wadleigh et al., 1994; Alewell et al., 2000). This confirms that SO_4^{2-} in shallow soils is mainly derived from precipitation, as pyrite has been almost completely removed from these weathered materials. At the catchment scale, the stream SO_4^{2-} is also dominantly derived from wet deposition, as stream SW has $\delta^{34}S_{SO4}$ values ∼3‰ (Table 3; Fig. 5B).

The sulfate concentrations of input fluxes (modern precipitation: 11 μM) is much lower than those of output fluxes (streams: 90 μM), suggesting net lost of S from the watershed. This is likely due to the slow release of sulfate that was loaded to the watershed during acid deposition in the northeastern US or/and dry deposition. A study at the Leading-Ridge forested watershed (less than 10 km from SSHO) reported five years of data (1979–1985) for sulfate export fluxes as river discharge as well as atmospheric wet sulfate deposition, and showed that input fluxes were much lower than output fluxes (Lynch and Corbett, 1989). Long-term monitoring at the well-characterized Hubbard Brook Experimental Forest had shown similar trends (Likens et al., 2002).

Given the oxic conditions observed in SSHO soils (Brantley et al., 2013), S that was deposited from acid rain has remained as sulfate instead of being reduced. $\delta^{34}S_{SO4}$ of groundwaters that have interacted with pyrite beneath the oxidation front should look like S from pyrite because S isotopes are negligibly fractionated during pyrite dissolution (Van Stempvoort et al., 1990; Mayer et al., 1995; Schiff et al., 2005). The S isotopes of the pyrite end-member were not directly measured, but framboidal pyrite has been observed in the Rose Hills shale bedrock under scanning electron microscope (Brantley et al., 2013). This indicates that pyrite in Rose Hill shale is formed during early diagenesis, and thus it has relatively low $\delta^{34}S$ values (Strauss, 1999). Indeed, some groundwaters have $\delta^{34}S$ as negative as −15‰, in the range of pyrite (Fig. 5B).

5.4. Acquisition of groundwater DIC in different flow pathways

The comparison among groundwater chemistries for the ten wells at SSHO suggests that the degree of ankerite dissolution and chemical evolution are generally higher moving towards the outlet of the catchment, although these wells are cased to about the same depth. Three distinct groups of water chemistry are observed among the sampled wells (Fig. 5B; Table 3): group 1 with low Ca^{2+} and high $\delta^{34}S_{SO4}$ values; group 2 with high Ca^{2+} and high $\delta^{34}S_{SO4}$ values; and group 3 with high Ca^{2+} and low $\delta^{34}S_{SO4}$ values. Similarly, Sr^{2+} concentrations and the ratios of Sr to divalent cations ($Ca^{2+} + Mg^{2+}$ concentrations) also group these groundwaters into the same three clusters (Fig. 5C). For example, the groundwaters with lower $\delta^{34}S_{SO4}$ values are characterized by higher $Sr^{2+}/(Ca^{2+} + Mg^{2+})$ ratios. The co-variation of $\delta^{34}S_{SO4}$ values and Ca^{2+} concentrations in groundwaters (Fig. 5B) is likely controlled by pyrite and ankerite dissolution. At the northern ridge of SSHO, where the entire weathering profile was sampled, the weathering fronts of pyrite and ankerite, were observed at almost

coincident depths (Jin et al., 2010). We attributed this coupling to the dissolution of pyrite that produces acidity and dissolves ankerite. If so, it is reasonable to observe higher Ca^{2+} (ankerite dissolution) and lower $\delta^{34}S_{SO4}$ values (pyrite dissolution) in group 3 along flow pathway 3 (Fig. 5A and B). Here, groundwater near the weir drains almost the entire catchment and has longer residence times. Groundwaters near the upper reach of the stream in group 1 have lower Ca^{2+} concentrations (no ankerite, flow pathway 1, Fig. 5A) and thus $\delta^{34}S_{SO4}$ values of acid rain (no pyrite). Here groundwaters discharging into the stream in the upper reach have only drained a small portion of the catchment and are characterized with a shorter residence time. Furthermore, a previous study on the Leading-Ridge watershed in central Pennsylvania has shown that during spring runoff, the water table rises quickly to the surface and almost the entire soil profile near the stream is saturated (Lynch and Corbett, 1989). During this time, solutes between unsaturated and saturated zones are displaced, leading to similar soil water and groundwater chemistry. However, some groundwaters near the outlet (group 2) are not falling on this trend. In these sites, groundwaters are characterized by carbonate dissolution (higher Ca^{2+} concentrations) but with S isotope signatures of wet deposition and lower $Sr^{2+}/(Ca^{2+} + Mg^{2+})$ ratios, following flow pathway 2. This observation suggests the decoupling of pyrite and ankerite dissolution fronts. One hypothesis to interpret this is presented below.

The negative saturation indices calculated for soil waters, groundwaters and streams from SSHO indicate carbonate unsaturation. However, a previous study showed that secondary carbonate may have precipitated at the valley floor soils at around 4 m below land surface of SSHO, as C isotopic composition of calcite at this site was different from that of the primary ankerite in the Rose Hills (Brantley et al., 2013; Table 1). The equilibrium fractionation factor between pedogenic calcite and soil CO_2 is approximately 8.4‰ at 25 °C (Clark and Fritz, 1997). Thus, given the observed range of $\delta^{13}C_{CO2}$ values through this work, the pedogenic carbonate ($\delta^{13}C_{Ca}$ of $-1.1‰$) proposed by Brantley et al. (2013) may not be formed recently; instead the carbonate could have precipitated before a mature forest was established when C4 vegetation dominated. Work is needed to test this hypothesis and understand the precipitation kinetics and controls on secondary calcite.

It can be assumed that weathering fronts of ankerite and pyrite are much deeper than a few meters and thus groundwaters collected near the outlet are dissolving secondary calcite, but not pyrite or ankerite (Fig. 5A). This hypothesis is consistent with Sr systematics in these groundwaters: presumably primary ankerite dissolution yields much higher $Sr^{2+}/(Ca^{2+} + Mg^{2+})$ ratios (pathway 3) than those from secondary calcite dissolution (pathway 2) (Fig. 5). This agrees well with the distribution coefficients observed for Sr in calcite, such that Sr prefers to remain in solution instead of substituting Ca in secondary mineral phases like pedogenic calcite (e.g., Mucci and Morse, 1983; Gabitov and Watson, 2006; Gabitov et al., 2014).

5.5. Controls on stream water C isotopes and DIC: mixing of groundwater and soil water?

As shown in Rxn (1) and Rxn (2) and also discussed in many research papers, stream chemistry alone cannot be used to differentiate silicate versus carbonate dissolution in watersheds of mixed lithology or mineralogy (e.g., Gaillardet et al., 1999; Tipper et al., 2006). At SSHO, the chemical weathering reactions have completely depleted ankerite, the carbonate mineral, in the soils and saprock, allowing us to investigate silicate mineral dissolution which dominates at shallow depths and carbonate dissolution at depth in the groundwaters. As discussed earlier, the $\delta^{13}C_{DIC}$ values and Ca^{2+} concentrations define the predominant weathering reactions in the SSHO: low Ca^{2+} and relatively low, but variable, $\delta^{13}C_{DIC}$ values are controlled by silicate dissolution in the presence of soil CO_2 in shallow soils and (carbonate-depleted) saprock; however, higher Ca^{2+} and constant but higher $\delta^{13}C_{DIC}$ values are attributed to ankerite dissolution at depth near the saprock–bedrock interface (Fig. 4B). The depth of this interface varies throughout the catchment from 23 meters beneath the northern ridge to 3 meters beneath the outlet of the catchment. Stream water chemistry is controlled by mixing of soil water (dominated by silicate dissolution) and groundwater (impacted by carbonate dissolution). More interestingly, the stream water becomes more concentrated in Mg^{2+} and Ca^{2+} downstream, probably as a result of hydrological control. For example, the stream towards the outlet receives a higher contribution from groundwater relative to shallow soil water. Studies on a few small watersheds have shown that DOC and DIC in streams vary considerably between flooding versus low-flow conditions (e.g., Andrews et al., 2011; Lloret et al., 2011). This has been attributed to differences in carbon contents of the contributions from surface runoff versus shallow groundwater (Lloret et al., 2011). Alternatively, the groundwater is more concentrated in Mg and Ca towards the outlet, so stream water towards the outlet could be more concentrated even if the relative contributions from soil water and groundwater remain the same along the stream. The groundwater chemistry data support the latter hypothesis (Fig. 4B).

The $\delta^{13}C_{DIC}$ values of the stream collected at the three sampling locations also evolve towards the groundwater end-member values moving from headwater downstream. The observation that $\delta^{13}C_{DIC}$ values along the stream are different suggests that carbon isotope ratios of soil water or groundwater and their relative contributions are the primary controls of stream $\delta^{13}C_{DIC}$. Other studies have made similar observations. For example, Kanduc et al. (2007) and Zavadlav et al. (2013) studied a karst drainage area of Sava (Slovenia), and concluded that riverine $\delta^{13}C_{DIC}$ were controlled mainly by carbonate weathering with high DIC. Similarly, in the Arcachon lagoon catchment of France, constant $\delta^{13}C_{DIC}$ values around $-20‰$ were observed throughout the year for the streams, pointing to the constancy of terrestrial organic carbon and silicate weathering as the DIC carbon sources (Polsenaere et al., 2013). In summary, case studies including ours at Shale

Hills have shown that mineral dissolution is the primary controls on riverine $\delta^{13}C_{DIC}$ values.

A few other secondary controls on the river water $\delta^{13}C_{DIC}$ values may also be important, including equilibration with the atmosphere, CO_2 degassing, and in-situ riverine biological processes (e.g., Parker et al., 2010). In some catchments, for example, equilibration with the atmosphere is observed to increase $\delta^{13}C_{DIC}$ values of streams. For example, atmospheric exchange was promoted by the presence of dams and lakes in Patagonian rivers of Argentina, and in that system the $\delta^{13}C_{DIC}$ values varied little despite seasonal changes (Brunet et al., 2005). Even at the outlet, the SSHO stream is still far from equilibrium with the atmosphere with respect to its C isotope composition (Fig. 5A). This is likely explained by: (1) the short length of the stream and short water residence time in the stream (stream length $\sim$ 300 m), and (2) the continual discharge of high pCO_2 groundwater into the stream, maintaining the stream far from equilibrium with the atmosphere as evidenced by major elemental chemistry. Equilibration of a stream can occur over long distances: for example, monitoring in the Pinal Creek (Arizona) showed that CO_2 gas-exchange continued to increase stream pH over 3 km downstream from a groundwater input point (Choi et al., 1998). Based on the AZ data, degassing is a relatively slow process, and equilibration is unlikely over the 300 m stretch of stream at SSHO.

Consistent with these conclusions, the pCO_2 of stream waters (ranging from 700 to 7500 ppm) calculated from pH and DIC is generally lower than those of soil water (ranging from 1700 to 34,000 ppm) or groundwater (ranging from 2600 to 49,000 ppm) but higher than atmospheric CO_2. Thus it is reasonable to assume that CO_2 begins degassing from the groundwater underlying the valley (Table 3). Indeed, the pCO_2 of the stream decreased slightly from the headwater (SH) to the outlet (SW) (Table 3). At the pH range observed in streams at SSHO (4.5–7.0), the dominant DIC species is H_2CO_3, and thus the measured $\delta^{13}C_{DIC}$ values can be approximately interpreted as $\delta^{13}C_{H2CO3}$. The fractionation factor between $CO_2(aq)$ (namely $H_2CO_3^*$) and $CO_2(gas)$ is small, $\sim$1.1‰ (Clark and Fritz, 1997); thus we do not expect significant C isotope shifts in the stream $\delta^{13}C_{DIC}$ due to degassing.

Enhanced photosynthesis in rivers can also consume CO_2, preferentially removing ^{12}C-rich carbon and leaving the remaining DIC with higher $\delta^{13}C_{DIC}$ values. For example, a study of the upper Danube River and its tributaries revealed that impounded reservoirs increased the transit time of water and allowed photosynthesis to increase the $\delta^{13}C_{DIC}$ values (Pawellek and Veizer, 1994). Indeed, monitoring of riverine $\delta^{13}C_{DIC}$ over 1000 km in Upper Danube river shows showed slow CO_2 degassing and changes in $\delta^{13}C_{DIC}$ downstream due to the oxidation of organic matter (Pawellek and Veizer, 1994). At the SSHO, the DOC concentrations in the first-order ephemeral stream increased dramatically in late summer, and was "attributed to processes in the stream itself such as in-stream processing (such as leaching and decomposition of allochthonous particulate organic matter and release by stream algae)" (Andrews et al., 2011). However, in the rest of the year, the stream

was observed to be well connected to shallow soil waters from the hillslopes, especially during high-flow conditions. During those periods, DOC is mainly contributed from soils (Andrews et al., 2011). For this study where sampling was completed in the high-flow seasons of November and April, it is unlikely that C isotope fractionation due to in-situ riverine photosynthesis was significant.

In summary, all of the evidence cited here is best explained by the conclusion that water in the first-order stream at SSHO is primarily derived from mixing of the soil water and carbonate-dissolution impacted groundwaters. Stream water $\delta^{13}C_{DIC}$ values are controlled by the isotopic signature of these two end-members as dictated by their relative contributions during different flow conditions.

5.6. CO_2 consumption potential of gray shale weathering

Shale weathering can release CO_2 by decomposition of fossil organic matter and consume CO_2 by dissolution of silicate and carbonate minerals. Below we presented a simple calculation to estimate the carbon mass balance of these processes. The first contribution is a small one: the CO_2 release rate by fossil OC degradation was calculated to be 1.3 mol m^{-2} kyr^{-1} as shown in Eqn. (1) (Table 4).

The second contribution, the consumption of atmospheric CO_2 by silicate dissolution, is estimated using two methods. As ankerite is completely depleted from the soils, we can assume soil water chemistry is solely controlled by silicate dissolution (after correction for contributions from wet precipitation). With this assumption, each mole of Ca^{2+} or Mg^{2+} that is solubilized by silicate dissolution is equivalent to one mole of CO_2 drawdown. The CO_2 consumption rate was roughly calculated as:

$$([Ca^{2+} + Mg^{2+}]_{SoilWater} - 2[Ca^{2+} + Mg^{2+}]_{ppn}) * D$$
$$= (103 - 8) \text{ μmol L}^{-1} * 53.5 \text{ cm yr}^{-1}$$
$$= 44 \text{ mol m}^{-2} \text{ kyr}^{-1} \qquad (3)$$

Here ($[Ca^{2+} + Mg^{2+}]_{SoilWater}$) is the sum of average soil water Ca^{2+} and Mg^{2+} concentrations observed at the deepest lysimeters (Table 4). The $[Ca^{2+} + Mg^{2+}]_{ppn}$ is the sum of average rainwater Ca^{2+} and Mg^{2+} concentrations at the two NADP sites (Table 4). As half of the rainfall is evapotranspired and thus the rainwater becomes concentrated by a factor of 2. An important assumption is that silicate dissolution becomes insignificant below soils and at depths above the reaction front for ankerite. This is very likely given that (1) silicate dissolution at soil waters already moves the system closer to silicate equilibrium and thus reaction slows down (e.g., Zhu, 2005; Jin et al., 2008) and (2) the pH of the groundwater is near neutral where clay dissolution is the slowest according to compiled experimental data (Brantley et al., 2008).

As a comparison, we can calculate the CO_2 flux transported by soil waters at 10°C (Table 4):

$$F_{H_2CO_3^*} = pCO_2 * K_{CO2} * D$$
$$= 40,000 \text{ ppm} * 10^{-1.47} * 53.5 \text{ cm yr}^{-1}$$
$$= 72 \text{ mol m}^{-2} \text{ kyr}^{-1} \qquad (4)$$

Here $[H_2CO_3^*]$ (or $[DIC]_{eq}$) is dissolved CO_2 concentrations, as controlled by its equilibrium with soil pCO_2 (K_{CO2} as Henry's Law constant). This is the maximum CO_2 flux moving to the groundwater by soil waters. This value is higher than the estimate based only on divalent cation concentrations but on the same order of magnitude. Importantly, this CO_2 dissolved in the soil water will be utilized during carbonate dissolution at depth as discussed below.

Given that two moles of CO_2 are consumed by one mole of ankerite dissolution (Rxn. (2)), the long-term rate of consumption of CO_2 out of the atmosphere can be calculated using ankerite depletion rates:

$$F_{ankerite} = C_{ankerite} * P * \rho_P / MW_{ankerite}$$
$$= 42 \text{ mol m}^{-2} \text{ kyr}^{-1} \qquad (5)$$

Eq. (5) is in principle similar to Eqn. (1) and Eqn. (2). Here, $C_{ankerite}$ is wt% of ankerite in Rose Hill bedrock, and $MW_{ankerite}$ is molecular weight of ankerite.

Similar to silicate dissolution rates, the CO_2 consumption rates from carbonate dissolution can be compared to those estimates based on divalent cation concentrations. In this exercise, the stream Ca and Mg concentrations ($[Ca^{2+} + Mg^{2+}]_{stream}$) are assumed to be from rain, silicate or carbonate dissolution, and soil water Ca and Mg concentrations ($[Ca^{2+} + Mg^{2+}]_{soilwater}$) are good estimates of contribution from rain and silicate dissolution (Eqn. (3)). Thus the CO_2 consumption rates by carbonate dissolution are:

$$F_{ankerite} = ([Ca^{2+} + Mg^{2+}]_{stream} - [Ca^{2+} + Mg^{2+}]_{soilwater}) * D$$
$$= (194 - 103)\mu M * 53.5 \text{ cm yr}^{-1}$$
$$= 48 \text{ mol m}^{-2} \text{ kyr}^{-1} \qquad (6)$$

This stream-derived CO_2 consumption rate by carbonate dissolution is a short-term average, and is very similar to the long-term CO_2 consumption rate estimated using rock chemistry based on Eqn (5). The contribution of protons from other species such as sulfuric acid contributed by pyrite dissolution is negligible for the whole catchment, as stream sulfate has similar $\delta^{34}S_{SO4}$ values compared to wet deposition (Fig. 4D).

This first-order estimate clearly shows that consumption of CO_2 by silicate mineral dissolution is as important as consumption by carbonate dissolution and is much larger than the CO_2 production rate from ancient OC degradation. Therefore, weathering of Rose Hill shale in this catchment is a sink for atmospheric CO_2 and is a net exporter of DIC to the larger Shavers creek watershed. Furthermore, our work on the Rose Hill shale as well as other studies in the literature document that reactions with organic matter and carbonates in shales occur quickly, often proceeding toward completion in the saprock beneath the soil in climates where precipitation exceeds evapotranspiration (Petsch et al., 2005; Jin et al., 2013; Brantley et al., 2013). These deep reactions occur as oxygenated and CO_2-charged fluids advect downward along fractures in the shale: the reaction with CO_2 is fast and is likely limited only by the mineral–water interfacial area.

Besides DIC, DOC can be an important component of the dissolved carbon budget that is transported out of a catchment (Amiotte-Suchet et al., 2007; Lloret et al., 2011). As discussed the majority of DOC in the stream is from degradation of modern vegetation in soils or riverine biological processes, with little to no contribution from the ancient organic matter in the Rose Hill formation. Further studies are needed to quantify this flux.

6. CONCLUSIONS AND IMPLICATIONS

This study has examined all major carbon reservoirs in a well-studied first-order catchment and evaluated the potential of gray shale to take up atmospheric CO_2 during shale alteration. We focused on two aspects of the C cycle: consumption of CO_2 by silicate versus carbonate dissolution and release of CO_2 by degradation of ancient organic matter.

Our results document that degradation of Silurian organic matter releases CO_2 at a rate of ~ 1 mol m^{-2} ky^{-1}. The CO_2 efflux from soil to atmosphere (measured at 7 sites along a planar transect between 2009 and 2011) is on the order of 1 μmol m^{-2} s^{-1}, or 31,500 mol m^{-2} kyr^{-1}. Thus, soil CO_2 is derived almost exclusively from C in the atmosphere or degradation of modern vegetation. Soil water dissolves silicate minerals (clays and plagioclase) while maintaining relatively low DIC (<100 μmol/L) in equilibrium with CO_2 in the soil atmosphere. Above the depth where carbonate minerals are encountered in the subsurface (3 m below land surface at valley floor) the shallowest groundwater behaves similarly to the soil waters. At deeper depths where groundwater is exposed to carbonate minerals such as primary ankerite or secondary calcite, DIC concentrations in groundwaters increase to ~ 2500 μmol/L, approaching chemical equilibrium with carbonate. The $\delta^{13}C_{DIC}$ values of these groundwaters are consistent with 1:1 mixing of the carbonate and soil CO_2 to the groundwater DIC. The S isotope data is consistent with the release of sulfuric acid due to pyrite dissolution in the bedrock beneath the ankerite dissolution front, but this S is minor when compared to the contribution of S to the stream that is derived from wet deposition in the whole catchment.

The net result of weathering in the SSHO is that the rates of carbonate dissolution and silicate dissolution are similar – ~ 40 mol CO_2 m^{-2} ky^{-1} – and are much higher than the estimated CO_2 release rates contributed by ancient organic matter oxidation (~ 1 mol CO_2 m^{-2} ky^{-1}). Importantly, the depths at which carbonates and silicates dissolve are vastly different in the catchment and are dictated by the overall relief (~ 30 m from northern ridge to valley floor) and the depth to the water table. Specifically, carbonates dissolve near the water table – more than 20 m deep under the ridgeline and 3 meters deep under the valley floor. In contrast, silicates dissolve mostly in the fractured rocks that comprise the upper 5 meters of the catchment. Thus, to understand the total impact of weathering of shale in this temperate climate requires not only analysis of soils but also the reaction fronts at depth.

REFERENCES

Alewell C., Mitchell M. J., Likens G. E. and Krouse H. R. (2000) Assessing the origin of sulfate deposition at the Hubbard Brook experimental forest. *J. Environ. Qual.* **29**, 759–767.

Allison C.E., Francey R.J. and Krummel P.B. (2003) $\delta^{13}C$ in CO_2 from sites in the CSIRO Atmospheric Research GASLAB air sampling network, (April 2003 version). In Trends: *A Compendium of Data on Global Change*. Carbon Dioxide Information Analysis Center, Oak Ridge National Laboratory, U.S. Department of Energy, Oak Ridge, TN, U.S.A.

Amiotte-Suchet P., Probst J. and Ludwig W. (2003) Worldwide distribution of continental rock lithology: Implications for the atmospheric/soil CO_2 uptake by continental weathering and alkalinity river transport to the oceans. *Global Biogeochem. Cycles* **17**, 1038. http://dx.doi.org/10.1029/2002GB001891.

Amiotte-Suchet P., Linglois N., Leveque J. and Andreux F. (2007) ^{13}C composition of dissolved organic carbon in upland forested catchments of the Morvan Mountains (France): influence of coniferous and deciduous vegetation. *J. Hydrol.* **335**, 354–363.

Andrews D. M., Lin H., Zhu Q., Jin L. and Brantley S. L. (2011) Hot spots and hot moments of dissolved organic carbon export and soil organic carbon storage in the Shale Hills Critical Zone Observatory. *Vadose Zone J.* **10**, 943–954. http://dx.doi.org/10.2136/vzj2010.0149.

Beaulieu, Goddéris E. Y., Labat D., Roelandt C., Calmels C. and Gaillardet J. (2011) Modeling of water-rock interaction in the Mackenzie basin: competition between sulfuric and carbonic acids. *Chem. Geol.* **289**, 114–123.

Benkovitz C. M., Scholtze C. M., Pacyna J., Tarrason L., Dignon J., Voldner E. C., Spiro P. A., Logan J. A. and Graedel T. E. (1996) Global gridded inventories of anthropogenic emissions of sulfur and nitrogen. *J. Geophy. Res.* **101**, 29239–29253.

Berner E. K. and Berner R. A. (1996) *Global Environment: Water, Air, and Geochemical Cycles*. Prentice-Hall, p. 376.

Boström B., Comstedt D. and Ekblad A. (2007) Isotope fractionation and ^{13}C enrichment in soil profiles during the decomposition of soil organic matter. *Oecologia* **153**, 89–98.

Brantley S. L., Holleran M. E., Jin L. and Bazilevskaya E. (2013) Probing chemical reactions underlying the Shale Hills Critical Zone Observatory, Pennsylvania (U.S.A.): nested weathering reaction fronts. *Earth Surf. Proc. Land.*. http://dx.doi.org/10.1002/esp.3415.

Brantley S. L., Kubicki J. D. and White A. F. (2008) *Kinetics of water–rock interaction*. Springer Science + Business Media, LLC, p. 833.

Brunet F., Gaiero D., Probst J. L., Depetris P. J., Lafaye F. G. and Stille P. (2005) $\delta^{13}C$ tracing of dissolved inorganic carbon sources in Patagonian rivers (Argentina). *Hydrol. Process.* **19**, 3321–3344.

Calmels D., Gaillardet J., Brenot A. and France-Lanord C. (2007) Sustained sulfide oxidation by physical erosion processes in the Mackenzie River Basin: climatic perspectives. *Geology* **35**, 1003–1006.

Cambell A. R. and Lueth V. W. (2008) Isotopic and textural discrimination between hypogene, ancient supergene, and modern sulfates at the Questa Mine, New Mexico. *Appl. Geochem.* **23**, 308–319.

Canfield D.E. (2001) Biogeochemistry of sulfur isotopes. In *Stable Isotope Geochemistry* (eds. J.W. Valley and D.R. Cole), vol. 43. Mineralogical Society of America, Blacksburg, VA. pp. 607–636.

Cerling T. E., Solomon D. K., Quade J. and Borman J. R. (1991) On the isotopic composition of carbon in soil carbon dioxide. *Geochim. Cosmochim. Acta* **55**, 3403–3405.

Choi J., Hulseapple S. M., Conklin M. H. and Harvey J. W. (1998) Modelling CO_2 degassing and pH in a stream-aquifer system. *J. Hydrol.* **209**, 297–310.

Clark I. D. and Fritz P. (1997) *Environmental Isotopes in Hydrogeology*. Lewis Publishers, New York, p. 328.

Clayton J. L. and Swetland P. J. (1978) Subaerial weathering of sedimentary organic matter. *Geochim. Cosmochim. Acta* **42**, 305–312.

Copard Y., Amiotte-Suchet P. and Di-Giovanni C. (2007) Storage and release of fossil organic carbon related to weathering of sedimentary rocks. *Earth Planet. Sci. Lett.* **258**, 345–357.

Edmond J. M. (1970) High precision determination of titration alkalinity and total carbon dioxide content of sea water. *Deep-Sea Res.* **17**, 737–750.

Ehleringer J. R., Sage R. F., Flanagan L. B. and Pearcy R. W. (1991) Climate change and the evolution of C_4 photosynthesis. *Trends Ecol. Evol.* **6**, 95–99.

Ekblad A., Nyberg G. and Ho□gberg P. (2002) ^{13}C-discrimination during microbial respiration of added C3-, C4- and ^{13}C-labelled sugars to a C3-forest soil. *Oecologia* **131**, 245–249.

Fitzgerald J. W. (1976) Sulfate ester formation and hydrolysis: a potentially important yet often ignored aspect of the sulfur cycle of aerobic soils. *Bacteriol. Rev.* **40**, 698–721.

Folk R. L. (1960) Peterography and origin of the Tuscarora, Rose Hill, and Keefer formations, lower and middle Silurian of eastern west Virginia. *J. Sediment. Petrol.* **30**, 1–58.

Friedli H., Lotscher H., Oeschger H., Siegenthaler U. and Stauffer B. (1986) Ice core record of the $^{13}C/^{12}C$ ratio of atmospheric CO_2 in the past two centuries. *Nature* **324**, 237–238.

Gabitov R. I. and Watson E. B. (2006) Partitioning of strontium between calcite and fluid. *Geochem. Geophys. Geosyst.* **Q11004**. http://dx.doi.org/10.1029/2005GC001216.

Gabitov R. I., Sadekov A. and Leinweber A. (2014) Crystal growth rate effect on Mg/Ca and Sr/Ca partitioning between calcite and fluid: an in-situ approach. *Chem. Geol.* **367**, 70–82.

Gaillardet J., Dupre B., Louvat P. and Allegre C. J. (1999) Global silicate weathering and CO_2 consumption rates deduced from the chemistry of large rivers. *Chem. Geol.* **159**, 3–30.

Gieskes J. M. and Roders W. C. (1973) Alkalinity determinations in interstitial waters of marine sediments. *J. Sediment. Petrol.* **43**, 272–277.

Graham C. and Lin H. (2011) Controls and frequency of preferential flow occurrence: a 175-event analysis. *Vadose Zone J.* **10**, 816–831. http://dx.doi.org/10.2136/vzj2010.0119.

Hamilton S. K., Kurzman A. L., Arango C., Jin L. and Robertson G. P. (2007) Evidence for carbon sequestration by agricultural liming. *Global Biogeochem. Cycles* **21**, GB2021, doi:10.1029/2006GB002738.

Hasenmueller E. A., Jin L., Smith L. A., Kaye M. W., Lin H., Brantley S. L. and Kaye J. P. (2014) Topographic controls and soil depth impacts on soil CO_2 concentrations and effluxes in a small temperate watershed. *Rev. Biogeochem.*.

Hedges J. I. and Oades J. M. (1997) Comparative organic geochemistries of soils and sediments. *Org. Geochem.* **27**, 319–361.

Hélie J., Hillaire-Marcel C. and Rondeau B. (2002) Seasonal changes in the sources and fluxes of dissolved inorganic carbon through the St. Lawrence River-isotope and chemical constraint. *Chem. Geol.* **186**, 117–138.

Herndon E. M., Jin L. and Brantley S. L. (2011) Soils reveal widespread Manganese enrichment from industrial inputs. *Environ. Sci. Technol.* **45**(1), 241–247.

Herut B., Zohary T., Krom M. D., Fauzi R., Mantoura C., Pitta P., Psarra S., Rassoulzadegan F., Tanaka T. and Thingstad T. F. (2005) Response of East Mediterranean surface water to Saharan dust: on-board microcosm experiment and field observations. *Deep-Sea Res. II* **52**, 3024–3040.

Hillaire-Marcel C. (1986) Isotopes and food. Chapter 12. In *Handbook of Environmental Isotope Geochemistry, vol. 2, The Terrestrial Environment, B.* (eds. P. Fritz and J.-Ch. Fontes). Elsevier, Amsterdam, The Netherlands, pp. 507–548.

Holland H. D. (1978) *The Chemistry of the Atmosphere and Oceans.* John Wiley and Sons, New York, p. 351.

Jaffe L. A., Peucker-Ehrenbrink B. and Petsch S. T. (2002) Mobility of rhenium, platinum group elements and organic carbon during black shale weathering. *Earth Planet. Sci. Lett.* **198**, 339–353.

Jahne B., Heinz G. and Dietrich W. (1987) Measurement of the diffusion coefficients of sparingly soluble gases in water. *J. Geophys. Res.* **92**, 10767–10776.

Jin L., Andrews D. M., Holmes G. H., Lin H. and Brantley S. L. (2011) Opening the "black box": water chemistry reveals hydrological controls on weathering in the Susquehanna Shale Hills Critical Zone Observatory. *Vadose Zone J.* **10**, 928–942. http://dx.doi.org/10.2136/vzj2010.0133.

Jin L., Mathur R., Rother G., Cole D., Bazilevskaya E., Williams J., Carone A. and Brantley S. L. (2013) Evolution of porosity and geochemistry in Marcellus formation black shale during weathering. *Chem. Geol.* **356**, 50–63.

Jin L., Ogrinc N., Hamilton S. K., Szrmek K., Kanduc T. and Walter L. M. (2009) Inorganic carbon isotope systematics in soil profiles undergoing silicate and carbonate weathering (Southern Michigan, USA). *Chem. Geol.* **264**, 139–153.

Jin L., Ravella R., Ketchum B., Bierman P. R., Heaney P., White T. and Brantley S. L. (2010) Mineral weathering and elemental transport during hillslope evolution at the Susquehanna/Shale Hills Critical Zone Observatory. *Geochim. Cosmochim. Acta* **74**, 3669–3691.

Jin L., Williams E., Szramek K., Walter L. M. and Hamilton S. K. (2008) Silicate and carbonate mineral weathering in soil profiles developed on Pleistocene glacial drift (Michigan, USA): mass balances based on soil water geochemistry. *Geochim. Cosmochim. Acta* **72**, 1027–1042.

Kanduc T., Szramek K., Ogrinc N. and Walter L. M. (2007) Origin and cycling of riverine inorganic carbon in the Sava River watershed (Slovenia) inferred from major solutes and stable carbon isotopes. *Biogeochemistry* **86**, 137–154.

Karim A. and Veizer J. (2000) Weathering processes in the Indus River Basin: implications from riverine carbon, sulfur, oxygen and strontium isotopes. *Chem. Geol.* **170**, 153–177.

Keller C. K. and Bacon D. H. (1998) Soil respiration and georespiration distinguished by transport analyses of vadose CO_2, $^{13}CO_2$, and $^{14}CO_2$. *Global Biogeochem. Cycles* **12**, 361–372.

Khanna P. K., Prenzel J., Meiwes K. J., Urich B. and Matzner E. (1987) Dynamics of sulfate retention by acid forest soils in an acidic deposition environment. *Soil. Sci. Soc. Am. J.* **51**, 446–452.

Kharaka Y. K., Gunter W. D., Aggarwal P. K., Perkins E. H. and DeBraal J. D. (1988) SOLMINEQ.88: a computer program for geochemical modeling of water–rock interactions. *U. S. Geol. Surv.*.

Koutika L., Bartoli F., Andreux F., Cerri C. C., Burtin G., Choné T. and Philippy R. (1997) Organic matter dynamics and aggregation in soils under rain forest and pastures of increasing age in the eastern Amazon basin. *Geoderma* **76**, 87–112.

Krouse H.R. and Grinenko V.A. (1991) *Stable Isotopes: Natural and Anthropogenic Sulphur in the Environment.* p. 440.

Kump L. R. and Arthur M. A. (1999) Interpreting carbon-isotope excursions: carbonates and organic matter. *Chem. Geol.* **161**(1–3), 181–198.

Kuntz B., Rubin S., Berkowitz B. and Singha K. (2011) Quantifying solute transport behavior at the Shale Hills critical zone observatory. *Vadose Zone J.* **10**, 1–15, http:// dx.doi.org/ 10.2136/vzj2010.0130.

Li S. L., Calmels D., Han G., Gaillardet J. and Liu C. Q. (2008) Sulfuric acid as an agent of carbonate weathering constrained by delta C-13(DIC): examples from Southwest China. *Earth Planet. Sci. Lett.* **270**, 189–199.

Likens G. E., Driscoll C. T., Buso D. C., Mitchell M. J., Lovett G. M., Bailey S. W., Siccama T. G., Reiners W. A. and Alewell C. (2002) The biogeochemistry of sulfur at Hubbard Brook. *Biogeochemistry* **60**, 235–316.

Lin H. S. (2006) Temporal stability of soil moisture spatial pattern and subsurface preferential flow pathways in the Shale Hills Catchment. *Vadose Zone J.* **5**, 317–340.

Littke R., Klussmann U., Krooss B. and Leythaeuser D. (1991) Quantification of loss of calcite, pyrite, and organic matter due to weathering of Toarcian black shales and effects on kerogen and bitumen characteristics. *Geochim. Cosmochim. Acta* **55**, 3369–3378.

Lloret E., Dessert C., Gaillardet J., Alberic P., Crispi O., Chaduteau C. and Benedetti M. F. (2011) Comparison of dissolved inorganic and organic carbon yields and fluxes in the watersheds of tropical volcanic islands, examples from Guadeloupe (French West Indies). *Chem. Geol.* **280**, 65–78.

Lueth V. W., Rye R. O. and Peters L. (2005) "Sour gas" hydrothermal jarosite: ancient to modern acid-sulphate mineralization in the southern Rio Grande Rift. *Chem. Geol.* **215**, 339–360.

Lynch J.A. (1976) *Effects of Antecedent Soil Moisture on Storm Hydrographs.* Pennsylvania State University, University Park.

Lynch J.A. and Corbett E.S. (1985) Source-area variability during peak flow. In *J. Irrig. Drain. Div. Am. Soc. Civ. Eng* (eds. E.B. Jones and T.J. Ward). pp. 300–307. In *Watershed Management in the 1980s* (eds. E. Jones and T. Ward). ASCE, Reston, VA. pp. 300–307.

Lynch J. A. and Corbett E. S. (1989) Hydrologic control of sulfate mobility in a forested watershed. *Water Resour. Res.* **25**(7), 1695–1703.

Ma L., Chabaux F., Pelt E., Blaes E., Jin L. and Brantley S. L. (2010) Regolith production rates calculated with uranium-series isotopes at Susquehanna/Shale Hills Critical Zone Observatory. *Earth Planet. Sci. Lett.* **297**, 211–225.

Ma L., Jin L. and Brantely S. L. (2011) How mineralogy and slope aspect affect REE release and fractionation during shale weathering in the Susquehanna/Shale Hills Critical Zone Observatory. *Chem. Geol.* **290**, 31–49.

Ma, L., Konter, J., Sanchez, D., Herndon, E., Jin, L. and Brantley, S.L. (2014). Quantifying the signature of the industrial revolution from Pb concentrations and isotopes in Pennsylvania soils. In review for Anthropocene.

Mayer B., Fritz P., Prietzel J. and Krouse H. R. (1995) The use of stable sulfur and oxygen isotope ratios for interpreting the

mobility of sulfate in aerobic forest soils. *Appl. Geochem.* **10**, 161–173.

Migdisov A. A., Ronov A. B. and Grinenko V. A. (1983) The sulfur cycle in the lithosphere. In *The Global Biogeochemical Sulphur Cycles, SCOPE 19* (eds. M. V. Ivanov and J. R. Freney). John Wiley & Sons, Chichester, pp. 25–95.

Mook W. G., Bommerson J. C. and Staverman W. H. (1974) Carbon isotope fractionation between bicarbonate and gaseous carbon dioxide. *Earth Planet. Sci. Lett.* **22**, 169–176.

Mucci A. and Morse J. W. (1983) The incorporation of Mg^{2+} and Sr^{2+} into calcite overgrowths: influences of growth rate and solution composition. *Geochim. Cosmochim. Acta* **47**, 217–233.

National Oceanographic and Atmospheric Administration (NOAA) (2007) U. S. Divisional and Station Climatic Data and Normals, Asheville, N.C., U.S. Dept. of Commerce, National Oceanic and Atmospheric Administration.

Nordstrom D. K. (1982) The effect of sulfate on aluminum concentrations in natural waters: some stability relations in the system Al_2O_3–SO_3–H_2O at 298 K. *Geochim. Cosmochim. Acta* **46**, 681–692.

Parker S. R., Poulson S. R., Smith M. G., Weyer C. L. and Bates K. M. (2010) Temporal variability in the concentration and stable carbon isotope composition of dissolved inorganic and organic carbon in two Montana, USA rivers. *Aquat. Geochem.* **16**, 61–84. http://dx.doi.org/10.1007/s10498-009-9068-1.

Pawellek F. and Veizer J. (1994) Carbon cycle in the upper Danube and its tributaries: $^{13}C_{DIC}$ constraints. *Israel J. Earth Sci.* **43**, 187–194.

Petsch S. T., Berner R. A. and Eglinton T. I. (2000) A field study of the chemical weathering of ancient sedimentary organic matter. *Org. Geochem.* **31**, 475–487.

Petsch S. T., Edwards K. J. and Eglinton T. I. (2005) Microbial transformations of organic matter in black shales and implications for global biogeochemical cycles. *Palaeogeogr. Palaeoclimatol. Palaeoecol.* **219**, 157–170.

Petsch S. T., Eglinton T. I. and Edwards K. J. (2001) ^{14}C-dead living biomass: evidence for microbial assimilation of ancient organic carbon during shale weathering. *Science* **292**, 1127–1131.

Polsenaere P., Savoye N., Etcheber H., Canton M., Poirier D., Bouillon S. and Abril G. (2013) Export and degassing of terrestrial carbon through watercourses draining a temperate podzolized catchment. *Aquat. Sci.* **75**, 299–319.

Qu Y. and Duffy C. J. (2007) A semidiscrete finite volume formulation for multiprocess watershed simulation. *Water Resour. Res.* **43**, W08419. http://dx.doi.org/10.1029/2006WR005752.

Rajan S. S. S. (1978) Sulfate adsorbed on hydrous alumina, ligands displaced, and changes in surface charge. *Soil Sci. Soc. Am. J.* **42**, 39–44.

Raymond P. A. and Cole J. J. (2003) Increase in the export of alkalinity from North America's largest river. *Science* **302**, 88–91.

Reuss J.O. and Johnson D.W. (1986) Acid deposition and the acidification of soils and waters. In *Ecological Studies*, vol. 59. Springer, Berlin.

Ridgwell A. and Edwards U. (2007) Geological carbon sinks. In *Greenhouse Gas Sinks* (eds. D. Reay, N. Hewitt, J. Grace and K. Smith). pp. 74–97.

Rive K., Gaillardet J., Agrinier P. and Rad S. (2013) Carbon isotopes in the rivers from the Lesser Antilles: origin of the carbonic acid consumed by weathering reactions in the Lesser Antilles. *Earth Surf. Proc. Land.* **38**, 1020–1035.

Sageman B. B., Murphy A. E., Werne J. P., Staeten C. A., Hollander D. J. and Lyons T. W. (2003) A tale of shales: the relative roles of production, decomposition, and dilution in the accumulation of organic-rich strata, Middle-Upper Devonian, Appalachian basin. *Chem. Geol.* **195**, 229–273.

Sharpe W.E. and Drohan J. R. (1999) The effects of acidic deposition on aquatic ecosystems in Pennsylvania. In *Proceedings of the 1998 Pennsylvania Acidic Deposition Conference*, vol. II. Environmental Resources Research Institute, University Park, PA.

Singh S. K., Sarin M. M. and France-Lanord C. (2005) Chemical erosion in eastern Himalaya: major ion composition of the Brahmaputra and ^{13}C of dissolved inorganic carbon. *Geochim. Cosmochim. Acta* **69**, 3573–3588.

Strauss H. (1999) Geological evolution from isotope proxy signals-sulfur. *Chem. Geol.* **161**, 89–101.

Stumm W. and Morgan J. J. (1996) *Aquatic Chemistry*, 3rd ed. Wiley-Interscience, New York.

Szramek K., McIntosh J. C., Williams E. L., Kanduc T., Ogrinc N. and Walter L. M. (2007) Relative weathering intensity of calcite vs. dolomite in carbonate-bearing temperate zone watersheds: carbonate geochemistry and fluxes from catchments within the St. Lawrence and Danube River Basin. *Geochem. Geophys. Geosyst.* **8**, Q04002, doi: 10.1029/2006GC001337.

Telmer K. and Veizer J. (1999) Carbon fluxes, pCO_2, and substrate weathering in a large northern river basin, Canada: carbon isotope perspectives. *Chem. Geol.* **159**, 61–86.

Thomas E., Lin H., Duffy C., Sullivan P., Holmes G. H., Brantley S. and Jin L. (2013) Spatiotemporal patterns of water stable isotope compositions at the Shale Hills Critical Zone Observatory: linkages to subsurface hydrologic processes. *Vadose Zone J.*. http://dx.doi.org/10.2136/vzj2013.01.0029.

Tipper E. T., Bickle M. J., Galy A., West A. J., Pomies C. and Chapman H. J. (2006) The short term climatic sensitivity of carbonate and silicate weathering fluxes: insights from seasonal variations in river chemistry. *Geochim. Cosmochim. Acta* **70**(11), 2737–2754.

Trumbore S. E. (2000) Constraints on below-ground carbon cycling from radiocarbon: the age of soil organic matter and respired CO_2. *Ecol. Appl.* **10**, 399–411.

Trust B. A. and Fry B. (1992) Stable sulphur isotopes in plants: a review. *Plant Cell Environ.* **15**, 1105–1110.

Ulrich B. and Pankrath J. (1983) *Effects of accumulation of air pollutants in forest ecosystems*. Redel, Dordrecht.

Van Stempvoort D. R., Reardon E. J. and Fritz P. (1990) Fractionation of sulfur and oxygen isotopes in sulfate by soil sorption. *Geochim. Cosmochim. Acta* **54**, 2817–2826.

Vogel J. C. (1993) Variability of carbon isotope fractionation during photosynthesis. In *Stable Isotopes and Plant Carbon–Water Relations* (eds. J. R. Ehleringer, A. E. Hall and G. D. Farquhar). Academic Press, San Diego, CA, pp. 29–38.

Wadleigh W. A., Schwarcz H. P. and Kramer J. R. (1994) Sulphur isotope tests of seasalt correction factors in precipitation: Nova Scotia, Canada. *Water Air Soil Pollut.* **77**, 1–16.

Williams E. L., Szramek K., Jin L., Ku T. C. W. and Walter L. M. (2007) The carbonate system geochemistry of shallow groundwater/surface water systems in temperate glaciated watersheds (Michigan, USA): significance of open system dolomite weathering. *Geol. Soc. Am. Bull.* **119**, 511–528. http://dx.doi.org/10.1130/B25967.1.

Wubbels J. K. (2010) Tree species distribution in relation to stem hydraulic traits and soil moisture in a mixed hardwood forest in central Pennsylvania. Master's Thesis, The Pennsylvania State University.

Wynn J. G., Bird M. I. and Wong V. N. L. (2005) Rayleigh distillation and the depth profile of $^{13}C/^{12}C$ ratios of soil organic carbon from soils of disparate texture in Iron Range National Park, Far North Queensland, Australia. *Geochim. Cosmochim. Acta* **69**, 1961–1973.

Yang C., Telmer K. and Veizer J. (1996) Chemical dynamic of the "St. Lawrence" riverine system: D_{H2O}, $^{18}O_{H2O}$, $^{13}C_{DIC}$, $^{34}S_{sulfate}$, and dissolved $^{87}Sr/^{86}Sr$. *Geochim. Cosmochim. Acta* **60**, 851–866.

Yesavage T., Fantle M. S., Vervoort J., Mathur R., Jin L., Liermann L. J. and Brantley S. L. (2012) Fe cycling in the Shale Hills Critical Zone Observatory, Pennsylvania: an analysis of microbiology, chemical weathering, and Fe isotope fractionation. *Geochim. Cosmochim. Acta* **99**, 18–38.

Zavadlav S., Kanduc T., McIntosh J. and Lojen S. (2013) Isotopic and chemical constraints on the biogeochemistry of dissolved inorganic carbon and chemical weathering in the Karst watershed of Krka River (Slovenia). *Aquat. Geochem.* **19**, 209–230.

Zhu C. (2005) In situ feldspar dissolution rates in an aquifer. *Geochim. Cosmochim. Acta* **69**, 1435–1453.

Associate editor: Andrew D. Jacobson